Theta-Gamma Coordination between Anterior Cingulate and Prefrontal Cortex Indexes Correct Attention Shifts

Benjamin Voloh

A THESIS SUBMITTED TO
THE FACULTY OF GRADUATE STUDIES
IN PARTIAL FULFILLMENT OF THE REQUIREMENTS
FOR THE DEGREE OF
MASTER OF SCIENCE

GRADUATE PROGRAM IN BIOLOGY
YORK UNIVERSITY
TORONTO, ONTARIO

June 2015

ABSTRACT

Anterior cingulate and prefrontal cortex (ACC/PFC) are believed to coordinate activity to flexibly prioritize the processing of goal-relevant over irrelevant information. This between-area coordination may be realized by common low frequency excitability changes synchronizing segregated high-frequency activations. This coordination hypothesis was tested by recording in macaque ACC/PFC during the covert use of attention cues. There were robust increases of 5-10Hz (theta) to 35-55Hz (gamma) phase-amplitude correlation between ACC and PFC during successful attention shifts but not unsuccessful ones. Cortical sites providing theta phases (1) showed a prominent cue induced phase reset, (2) were more likely in ACC than PFC, and (3) hosted neurons with burst firing events that synchronized to distant gamma activity. These findings suggest that inter-areal theta-gamma correlations could follow mechanistically from a cue-triggered reactivation of rule-memory that synchronizes theta across ACC/PFC.

DEDICATION

To my friends and family, your support is the world to me.

ACKNOWLEDGMENTS

First and foremost, I'd like to thank my supervisor, Dr Thilo Womelsdorf, for his unwavering support and guidance. I have learned so much about how to be a good scientist, and of the importance of being thoughtful, clear, and courageous in exploring new paths. I truly hope that we can continue to work together, regardless of where my path leads.

My family is a rock in my life, and I would be adrift without them.

Distance can bring clarity. To Katherine, thank you for reminding me that not every problem is a crisis, and that every crisis is an opportunity.

To my old friends, thank you for providing a necessary distraction, and reminding me of my impending doom.

To my new friends, and colleagues, ours is an exciting field, not least because of the people in it. Thank you for all your help and support. You're all special snowflakes.

I'd also like to thank Dr. Daniel Kaping, Johanna Stucke, Iman Janemi and Michelle Bale for their work in collecting this data. I'm indebted to your efforts.

STATEMENT OF CONTRIBUTION

The experiments were designed by Dr Stefan Everling of the Univeristy of Western Ontario and Dr Thilo Womelsdorf. Data was collected by Dr. Daniel Kaping, Johanna Stucke, Iman Janemi and Michelle Bale. For my graduate studies, I developed the hypothesis and analysis plan in conjunction with my supervisor. I was responsible for all analysis, excluding those pertaining to burst firing and firing rate, which were performed by Dr Thilo Womelsdorf. This included development of a MATLAB code pipeline, data analysis, the generation of figures and tables, and interpretation. As first author, I wrote the first draft of the manuscript and compiled all result figures, and was subsequently deeply involved in all revisions in conjunction with Dr Thilo Womelsdorf.

Benjamin Voloh **Thilo Womelsdorf**

TABLE OF CONTENTS

ABSTRACT ii
DEDICATION iii
ACKNOWLEDGMENTS iv
STATEMENT OF CONTRIBUTION v
TABLE OF CONTENTS vi
LIST OF TABLES ix
LIST OF FIGURES x
LIST OF EQUATIONS xi
LIST OF ABBREVIATIONS xii
CHAPTER 1: INTRODUCTION 1
1.1 - Anatomical substrate of attention 2
1.1.1 - ACC – Adjustment and modulation of task representation 3
1.1.2 - VMPFC – Value Representation and Decision Making 4
1.1.3 - LFPC – Implementing task rules 5
1.1.4 – Interactions between areas 5
1.2 - Oscillatory signatures of information coordination 6
1.3 - Hypothesis and Summary of Findings 8
CHAPTER 2: METHODS 10
2.1 - Electrophysiological recording and data acquisition. 10
2.2 - Behavioral task 11
2.3 - Anatomical reconstruction 12
2.4 - Definition of error trials 13
2.5 - Analysis of cross-frequency phase-amplitude correlations 14
2.6 - Analysis of cross-frequency interactions using Tort's Modulation Index. 15
2.7 - Analysis of cross-frequency interactions using the weighted Phase Locking Factor 15
2.8 - Testing for changes in cross frequency correlation. 16
2.9 - Statistical surrogate analysis of single LFP-pair cross-frequency correlation 16
2.10 - Temporal specificity of theta-gamma phase-amplitude correlation 17
2.11 - Controlling for differences in trial number between correct and error trials 17
2.12 - Analysis of the low frequency phases of gamma frequency correlation 18
2.13 - Anatomical specificity of theta-gamma phase amplitude correlation 19
2.14 - Relation of maximal gamma amplitude to cue-onset time and low frequency phase 21
2.15 - Relation of phase amplitude correlation to changes in LFP power 21
2.16 - Relation of phase amplitude correlation to theta phase 21
2.17 - Relation of phase amplitude correlation to the average field potential 22
2.18 - Relation of phase amplitude correlation to LFP phase synchronization 23
2.19 - Dissociating value and spatial information contribution to theta-gamma phase-amplitude correlation 24
2.20 - Quantifying attention information in the firing rate of recorded neurons 25

2.21 - Comparison of theta-gamma correlation of LFP-LFP pairs with the strength of burst-LFP synchronization **26**

CHAPTER 3: PHASE AMPLITUDE CORRELATION IN THE ACC & PFC **28**
3.1 - Attention cue triggers theta-gamma phase-amplitude correlations. **28**
3.2 - Theta-gamma correlations fail to emerge on error trials. **30**
3.3 - Inter-areal cross-frequency correlation is anatomically specific. **32**
3.4 - Cue induced theta-phase reset in LFPs showing theta-gamma correlation. **33**
3.5 - Selective theta-gamma correlation for target locations and reward value, and its relation to firing rate information. **34**

CHAPTER 4: THETA-GAMMA CORRELATION & SINGLE UNIT EVENTS **35**
4.1 - The relation of theta-gamma correlations and firing rate modulation during attention shifts **35**
4.1.1 - Relation of overall theta-gamma cross frequency correlation with the degree of firing rate information 37
4.1.2 - Relation of spatially specific theta-gamma cross frequency correlation with spatially specific firing rate information 39
4.1.3 - Relation of reward specific theta-gamma cross frequency correlation with reward specific firing rate information 40
4.2 - The relation of theta-gamma LFP-LFP correlations and burst-LFP synchronization **41**

CHAPTER 5: DISCUSSION & CONCLUSION **44**
5.1 - Discussion **44**
5.1.1 - Frequency specificity of phase-amplitude correlation in ACC/PFC. 45
5.1.2 - Functional significance of theta-phase resets in the ACC/PFC. 46
5.1.3 - Theta-gamma correlation as a means to coordinate attention information. 48
5.2 - Conclusion **50**

BIBLIOGRAPHY **54**

APPENDICES **61**
APPENDIX A: SUPPLEMENTARY RESULTS **61**
Result A1 - Results of LFP-LFP pairs from individual monkeys 61
1.1 – Theta-Gamma Correlation on Correct and Error trials 61
1.2 - Theta Phase Preferences for Gamma Amplitude Modulation 62
1.3 - Anatomical Distribution of Theta-Gamma Correlation 63
1.4 - Analysis of Theta Phase Reset 63
1.5 - Analysis of LFP Power 64
1.6 - Average Cue-aligned Field Effects 64
1.7 - Theta Frequency Phase Coherence Analysis 65
1.8 - Temporal Jitter of Gamma Amplitude Phase to Theta versus Cue Onset Time 65
1.9 - Comparison of Trial Number Matched Correct and Error Trials 65
Result A2 - Behavioral Analysis 65
Result A3 - Analysis of LFP pairs showing significantly reduced theta-gamma correlation following attention cue onset 67
Result A4 - Relation of cross-frequency correlations to LFP power modulation at theta and gamma frequency bands. 68
Result A5 - Relation of the gamma amplitude variations to the time of cue onset versus the phase of remote theta band fluctuations 69
Result A6 - Equalizing the number of correct and error trials using a randomization approach. 70

Result A7 - Accounting for differences of overall modulation strength of correct and error trials on phase preference 71
Result A8 - Testing for the effect of the average field potential to explain the difference of P-A correlation in correct versus error trials. 71
Result A9 - Testing global distribution of phase or amplitude LFPs 72
Result A10 - The relation of phase synchronization, phase resetting, and phase-amplitude correlation 72
Result A11 - Selectivity of theta-gamma correlation for the attended target location or reward outcome associated with the target location 74
11.1. Selectivity for spatial target location of attention. 75
11.2. Selectivity for the reward outcome associated with the attended target stimulus. 76
APPENDIX B: FIGURES & TABLES 78
Figures and Tables for Main Results 78
Figures and Tables for Supplementary Results 86

LIST OF TABLES

Table 1. The relationship of theta gamma phase amplitude correlation and burst-LFP synchroniation across all types of channel combinations 85

A1 Table 1. The distribution of preferred phases of coupling is significantly non-uniform for correct but not error trials 91

LIST OF FIGURES

Figure 1. Phase-amplitude interactions support phase precession 78
Figure 2. Task and illustration of example theta-gamma correlation 80
Figure 3. Theta-gamma correlation is significantly enhanced after attention cue onset on correct trials 81
Figure 4. Preferred theta phase of theta-gamma correlation on correct and error trials 82
Figure 5. Anatomical origins of cortical sites with phase and amplitude modulation during theta-gamma correlation 83
Figure 6. Phase providing LFPs engaging in significant theta-gamma correlation show a theta phase reset after attention cue onset on correct trials 84

Figure A1. Illustration of anatomical reconstruction of recording sites 87
Figure A2. Example LFP-LFP pairs showing theta-gamma correlation in the post-cue period 89
Figure A3. Theta-gamma correlation is significantly enhanced after attention cue onset on correct trials in a narrow theta-gamma range 90
Figure A4. Theta-gamma correlation indexed with Maris' weighted phase Locking Factor 92
Figure A5. Median power spectral densities for phase- and amplitude- providing LFP recordings 94
Figure A6. Phase synchronization in the phase-amplitude correlation network during the attention shift 95
Figure A7. Representation of spatial information and information about target associated reward outcome in theta-gamma phase-amplitude correlation 96
Figure A8. Cue triggered attention shifts during rule reactivation and remapping, and hypothetical dynamic circuit motif of theta-gamma P-A correlation 97

LIST OF EQUATIONS

Equation 1 15
Equation 2 15
Equation 3 16
Equation 4 16
Equation 5 19
Equation 6 20
Equation 7 25
Equation 8 25
Equation 9 26

LIST OF ABBREVIATIONS

Abbreviation	Full phrase	Definition
ACC	Anterior cingulate cortex	Brodmann area 24
LPFC	Lateral prefrontal cortex	Brodmann area 46, 9, 8
VMPFC	Ventromedial prefrontal cortex	Brodmann area 32, 10
CFC	Cross frequency correlation	Index of interaction between oscillations of different frequencies
P-A	Phase-amplitude	Denotes the interaction between the phase of one frequency and the amplitude of another
Pre-cue	Pre attention cue onset	Activity preceding the attention cue onset
Post-cue	Post attention cue onset	Activity following the attention cue onset

CHAPTER 1: INTRODUCTION

Albert Einstein once said “Any man who can drive safely while kissing a pretty girl is simply not giving the kiss the attention it deserves”. Of course, the pretty girl may be a distraction from the much more contextually relevant stop sign, or the salient police car emblazoned in red and blue. Such a scenario, enjoyable though it may be, actually represents an inability of our system to recognize and process salient environmental cues that benefit the organism, instead of distractors that harm. Had Einstein’s prefrontal cortex been functioning properly, he may have noticed the signs, and ignored the pretty girl until an appropriate time.

Although attention can be shifted in a bottom-up fashion by salient features (e.g. color), attention can be guided by more complex rules and associations, which is critically dependent on the prefrontal cortex (Miller and Buschman, 2013). Lesions of the prefrontal cortex destroy the ability of monkeys to shift attention cued by a learned stimulus, but does not impact their ability to detect changes in pop-out targets (Rossi et al., 2007), suggesting that the prefrontal cortex is critical specifically to the deployment of attention for higher-order (e.g. learned) relevance. Indeed, pathological conditions such as schizophrenia (Carter et al., 2010), and attention-deficit hyperactivity disorder (Bush, 2009) are defined by activity across the prefrontal cortex that is markedly different from healthy controls, with a concomitant decrease in behavioural measures of successful attentional deployment. Successful shifting of attention relies on mechanisms that can integrate goal-relevant, task dependent information across distributed neural networks that integrate diverse but relevant streams of information.

The aim of my Master’s thesis is to investigate how networks supporting attention shifts are formed. This work is embedded in a larger literature on oscillatory activity in the brain that supports various cognitive and computational demands (Varela et al., 2001; Buzsaki, 2006;

Lisman and Jensen, 2013). Oscillatory signatures of attention are prevalent in both lower and higher order areas (Womelsdorf and Fries, 2007; Gregoriou et al., 2009; Buschman et al., 2012; Liebe et al., 2012; Phillips et al., 2013; Cavanagh and Frank, 2014). Importantly, not only are different oscillations functionally relevant, but they can also interact in support of computational demands (Buschman et al., 2012; Lisman and Jensen, 2013). In the following, I will outline the anatomical substrate of attention, and review oscillatory signatures of attentional processing.

1.1 - Anatomical substrate of attention

The prefrontal cortex is a heterogeneous region located in the frontal lobe, which can be divided into many different sub-regions. It has been implicated in a wide array of functions, including maintenance of working memory, attentional allocation, learning, foraging, and planning (Passingham and Wise, 2012).

The PFC can be subdivided into various sub-regions by architectonics, the differentiation of cortical regions based on physiological measures such as cell type, cell size, cell density, and cell morphometry. The lateral PFC (LPFC) is composed of areas 8, 9, and 46 and is similar between monkeys and humans. However, humans have 3 sulci (inferior frontal sulcus, superior frontal sulcus, and frontal sulcus), whereas monkeys have just one (the principle sulcus) (Passingham and Wise, 2012). On the medial aspect is the ventromedial PFC (VMPFC; area 10 and 32) and the anterior cingulate cortex (ACC; area 24). There is an additional sulcus dorsal to area 32 that is present in some humans and great apes, but not in monkeys (paracingulate sulcus) (Passingham and Wise, 2012). The various areas are illustrated in **A1 Figure 1.**

In addition to architectonics, the PFC can be mapped according to function. Studies involving rule acquisition, representation, and selection have delineated specific roles localized in the PFC. The LPFC encodes task rules and deploys attention in support of task-relevant goals

(Passingham and Wise, 2012). The ACC monitors "self-generated actions" (Passingham and Wise, 2012) and their outcomes; activation of this area occurs when behavioral adjustments will be made (e.g. task rule- switching in response to an unexpected outcome). The VMPFC has been implicated in the encoding of stimulus values and evaluation of self-generated decision (Passingham and Wise, 2012).

1.1.1 - ACC – Adjustment and modulation of task representation

The ACC (area 24) has connections with the hippocampus, striatal structures, and other prefrontal areas, as well as with the amygdala (involved in processing reward and motivation). This connection facilitates updating of outcome valuations following actions (Passingham and Wise, 2012). In a task where monkeys had to switch between lifting or turning a joystick to obtain a reward, lesions in area 24 resulted in slower switching to new rules (Kennerley et al., 2006). In particular, these deficits were apparent for both positive and negative (i.e. correct and error) feedback. This implies that lesioned animals had problems persisting with a particular strategy, rather than in failing to process error feedback. In line with the study by Kennerly and colleagues, Rudebeck and colleagues showed that area 24 plays a role in action-outcome encoding, not stimulus (object)-outcome encoding (Rudebeck et al., 2008).

Activity in the ACC is responsive to prediction errors, where the observed outcome is different from the expected outcome (Yeung et al., 2004; Matsumoto et al., 2007), with distinct populations encoding either positive or negative errors. However, other cells in the ACC do not show this preference and rather encode the unsigned error (Hayden et al., 2011), suggesting ACC plays a role in monitoring outcomes. Thus, the function of the ACC is generally to evaluate the cost of implementing control, consistent with signals representing monitoring outcomes,

resolving conflicts, and detecting errors (Shenhav et al., 2013). This evaluative, or 'monitoring' function becomes evident during attention shifts ; when attention is shifted, ACC neurons encode the location and value of attentional target stimuli (Kaping et al., 2011). In other words, integrating (and resolving) conflicting information about potential attentional targets involves the ACC.

1.1.2 - VMPFC – Value Representation and Decision Making

Unlike area 24, which has connections with premotor areas as well as other prefrontal areas, area 32 is only indirectly connected to premotor areas (Passingham and Wise, 2012). It also receives input from the hippocampus, amygdala, and orbitofrontal circuits (Averbeck and Seo, 2008). In monkeys, area 32 has cells that encode target value with rapid onset latency following attention cues (Kaping et al., 2011; Rushworth et al., 2011). Whereas area 24 activates in response to monitoring stimulus choices, area 32 is involved in monitoring of outcome volatility (a function of reward magnitude and probability) (Behrens et al., 2007).

Neurons in area 10 encode the decision at the time of feedback, reflecting the monitoring/ evaluating of decisions (Tsujimoto et al., 2010a). There are few studies of area 10, and they seem to suggest that one of its core functions is learning based on single events (Passingham and Wise, 2012). Patients with lesions in the VMPFC (including its medial and frontal polar aspects) perform worse on the Iowa Gambling Task, a proxy for value-based decision making (Glascher et al., 2012). The unique anatomical and functional connectivity of the VMPFC as opposed to the ACC or the LPFC makes this area optimal for encoding of values for decisions.

1.1.3 - LFPC – Implementing task rules

The LPFC encodes goals and task-dependent rules that structure goal directed behavior (Glascher et al., 2012; Passingham and Wise, 2012). Lesions of the LPFC lead to decreased performance on the Stroop task, which evaluates the ability of our system to override automatic behavior in favor of cognitively demanding behavior (Glascher et al., 2012; Shenhav et al., 2013). This suggests that the LPFC is involved in maintaining stimulus-response relationships and strategic planning. This region also has strong connections to motor and parietal areas, both involved in planning movement goals (Passingham and Wise, 2012; Genovesio et al., 2014), and is thus well-positioned to modulate motor plans to achieve task goals.

1.1.4 – Interactions between areas

Whereas task-rules are encoded in the LPFC, it is likely that the ACC has a role in the selection of appropriate task rules when tasks are demanding enough to require it (Shenhav et al., 2013). Functional studies support this link. ACC and LPFC theta-band coherence increases following errors, and the degree of coherence predicts behavioral adjustments (Cavanagh et al., 2009). This suggests that the two structures coordinate to adjust behavior. Likewise, when learning with targets are rewarded, gamma band power increases in both ACC and LPFC, with the former preceding the latter (Rothé et al., 2011). Importantly, this lag is correlated only during explorations, and disappears when animals repeat the movement, consistent with a role for the ACC signaling a need for adjustment.

The anatomical segregation of functions among different brain areas requires a mechanism for transferring information across areas. Anatomical connections between LPFC, VMPFC, and ACC are strong, but each has unique inputs and outputs with subcortical and distal

cortical structures. At a local level, the cortex is highly interconnected, and communication with distant areas occurs via a relatively small number of long distance projections, occuring between areas of varying laminar types (Barbas, 2015). Thus, the coordination of information hosted in different sites requires a mechanism that can scale from local circuits to long-range / large-scale networks. Neuronal oscillations have characteristics suitable for such local-to-long range information transfer.

1.2 - Oscillatory signatures of information coordination

Across species, oscillatory activity emerges in relation to diverse behavioural states, including resting states, goal-oriented processing, and motor output (Buzsaki, 2006; Engel and Fries, 2010; Lisman and Jensen, 2013). Oscillations can be detected in electrophysiological recordings ranging in scale from single units to EEG. Recordings at different scales reflect different contributing electrical currents; for example, LFP recordings reflect changes in trans-membrane currents of 10s-1000s of neurons, with neurons closer to the electrode tip contributing more to the observed signal than those further away. Typically, oscillatory activity is evident in specific frequency bands, such as high gamma (60-100 Hz), low gamma (30-60 Hz), beta (15-30 Hz), alpha (10-15 Hz), theta (4-10 Hz), and delta (1-4 Hz). Rhythms are generally well-preserved across species, reflecting a need for the brain to keep time even as it grows (Buzsáki et al., 2013). Fast rhythms (>30 Hz) operate at a local level, because their short periods allow the integration of the activity relatively fewer neurons. On the other hand, slow oscillations (<30 Hz) are ideally suited to global operation because of their long periods, allowing for integration of the activity of a greater number of neurons (von Stein and Sarnthein, 2000; Varela et al., 2001).

Importantly, fast oscillations can be nested in slower ones, with important functional and mechanistic consequences. A rich set of predominantly rodent studies has documented that the

phase of lower frequencies modulates the amplitude of higher frequencies, so called phase-amplitude coupling (PA coupling; **Fig. 1A**) (Buzsaki, 2006; Canolty and Knight, 2010; Lisman and Jensen, 2013). Low frequencies may modulate local gamma activity in spatially segregated areas (Sirota et al., 2008; Schroeder and Lakatos, 2009; von Nicolai et al., 2014), activating local populations of neurons at different phases of the slower frequencies, which could support phase coding. This interaction has been used to explain the phenomenon of phase precession in rats (*see* **Fig. 1B**) (O'Keefe and Recce, 1993; Jensen and Colgin, 2007). Place cells in rat hippocampus encode a rat's location. When a rat moves through its environment, place cells fire earlier in an ongoing theta cycle as the rat moves through its preferred location (i.e. 'place field'). Importantly, place cells with different place fields tend to fire in different gamma cycles (Lisman and Jensen, 2013), suggesting the interaction between theta/gamma is instrumental. Reading out the trajectory of a rat by taking phase into account allows more accurate predictions then when theta phase is ignored (Huxter et al., 2008). Although oscilaltions are prevalent in the ACC and PFC, it is unclear if phase-amplitude coupling in the PFC and ACC exists, or whether it has a functional role.

Several lines of evidence suggest that band-limited, rhythmic activation at low and high frequency bands are used in primate ACC/PFC cortical circuits to implement higher cognitive functions (Buschman et al., 2012; Salazar et al., 2012; Womelsdorf et al., 2014b). In the low frequency range, a 5-10 Hz theta band has been shown to carry stimulus information during retention periods of working memory tasks (Liebe et al., 2012), to increase in strength when cognitive control demands increase (Womelsdorf et al., 2010) and when behavior is rewarded (Tsujimoto et al., 2006), to predict behavioral adaptation in response to errors (Cavanagh et al., 2010), and to phase couple to parietal cortices during goal-directed as opposed to habitual

behaviours (Phillips et al., 2013). These studies suggest that activity fluctuations in the theta band might organize internally generated representations of goal-relevant information. In principle, such representations could be used during enhanced processing demands to covertly decide which aspects of the environment should be attended. In addition to theta-band activity, distal gamma activity is also observed and is associated with increases in attentional demands (Gregoriou et al., 2009), and when feedback via errors signals a need for control (Rothé et al., 2011). In rodents studies, theta-nested sequences of spiking activity of many neurons carry significant information about the goal locations that rodents eventually will choose to explore (Colgin et al., 2009; Bieri et al., 2014). A hallmark of these internally-generated spiking events is not only their nesting in theta rhythmic fluctuations, but their co-occurrence with gamma band network activations (Colgin et al., 2009; Pezzulo et al., 2014). According to these findings, theta-gamma P-A correlations might provide a general signature that indexes when and how attention- and choice-relevant information is temporally organized and integrated around the time when a choice is made, or when attention covertly selects one stimulus' information against other, distracting stimuli (Pezzulo et al., 2014).

1.3 - Hypothesis and Summary of Findings

In light of the need for global coordination across the ACC and PFC for attentional deployment, I hypothesized that phase-amplitude interactions support covert control processes of attention and choice. Unlike most studies on cross-frequency interactions, I use the more careful term "phase-amplitude correlation" (instead of coupling) to highlight that our measure is purely correlational (Aru et al., 2015). To this end, I analyzed local field potential (LFP) activity at multiple sites in the ACC, VMPFC, and LPFC in two macaques performing a selective attention task (Kaping et al., 2011). The task paradigm used a cue to covertly shift attention to a relevant

instead of an irrelevant stimulus (**Fig. 2A**). The successful use of the cue to covertly shift visual attention was accompanied by reliable theta-gamma P-A correlations between medial and lateral prefrontal cortex. This inter-areal theta-gamma P-A correlation was absent on error trials and driven particularly by theta-phase providing LFPs from the ACC. Control analyses revealed that the functionally significant theta-gamma correlations were closely linked to an attention-cue induced theta-specific phase reset, but was unrelated to average (evoked) fields in the ACC/PFC, to spurious power variations, or to variations in inter-areal theta-band coherence.

CHAPTER 2: METHODS

The local field potential (LFP) recordings and anatomical reconstruction of recording sites reported in this manuscript are from the dataset and experiment described in detail by Kaping and colleagues (2011). All methods, including those pertaining to results in **Appendix A**, are described here for the sake of completeness.

2.1 - Electrophysiological recording and data acquisition.

I analyzed the local field potential (LFP) in two awake and behaving macaque monkeys in 102 experimental sessions (26 and 76 for monkeys M and R, respectively). These were recorded previously, described in detail in (Kaping et al., 2011) and following the guidelines of the Canadian Council of Animal Care policy on the use of laboratory animals and of the University of Western Ontario Council on Animal Care. In the present study, I analyzed a total of 344 LFPs and 1104 LFP pairs. Extra-cellular recordings commenced with 1-6 tungsten electrodes (impedance 1.2-2.2 MΩ, FHC, Bowdoinham, ME) through standard recording chambers (19mm inner diameter) implanted over the left hemisphere in both monkeys. Electrodes were lowered through guide tubes with software controlled precision microdrives (NAN Instruments Ltd., Israel) on a daily basis, through a recording grid with 1 mm inter-hole spacing. Before recordings began, anatomical 7T MRIs were obtained from both monkeys, visualizing possible electrode trajectories using iodine placed inside the recording grid within the chamber. Data amplification, filtering, and acquisition were done with a multi-channel processor (Map System, Plexon, Inc.), using headstages with unit gain.

The recording experiments were performed with the monkeys placed in a sound attenuating isolation chamber (Crist Instrument Co., Inc.) , sitting in a custom made primate

chair as they viewed visual stimuli on a computer monitor (85 Hz refresh rate, distance of 58 cm). The monitor covered 36º x 27º of visual angle at a resolution of 28.5 pixel/deg. Eye positions were monitored using a video-based eye-tracking system (ISCAN, Woburn, US, sampling rate: 120 Hz). Monkeys were calibrated prior to each experiment to a 5 point fixation pattern (one central fixation point and the remaining four points offset by vertical 8.8º and horizontal 6º toward the 4 corners of the monitor). Eye fixation was controlled within a 1.4-2.0 degree radius window. During the experiments, stimulus presentation, eye positions and reward delivery were controlled via the software MonkeyLogic (open-source software http://www.monkeylogic.net) running on a Pentium III PC (for details*, see* (Kaping et al., 2011)). Liquid reward was delivered by a custom made, air-compression controlled, mechanical valve system with a noise level during valve openings of 17 dB within the isolation chamber.

2.2 - Behavioral task

Monkeys performed a selective attention, 2-forced choice discrimination task (for details, *see* (Kaping et al., 2011)). The task involved 2 sec. intertrial intervals, before a small gray fixation point was presented centrally on the monitor. Monkeys had to direct their gaze and keep fixation onto that fixation point until the end of the trial. After 300 ms fixation, two black/white grating stimuli were presented to the left and right of the center and contained oblique movements of the grating within their circular aperture. After 400 ms each stimulus changed color to either black/red or black/green. After a variable time (50 750 ms) the color of the central fixation point changed to either red or green, which cued the monkeys to covertly shift attention towards the location where the color of the grating matched the color of the fixation point. Monkeys maintained central fixation *and* sustained covert peripheral attention on the cued stimulus until it underwent a transient clockwise or counter-clockwise rotation, ignoring possible

rotations of the non-attended (uncued) stimulus, which occurred in 50% of the trials. To obtain a liquid reward, the monkeys had to discriminate the rotation by making up- or downward saccades for clockwise /counter-clockwise rotations (the mapping was reversed between monkeys). Following this choice and a 400 ms waiting period the animals received fluid reward. In the majority of experimental sessions (including experimental sessions and sessions with at least one LFP that was in ACC/PFC, 70 of 80 sessions of monkey R, and 70 of 73 sessions of monkey M) the magnitude of the fluid reward varied as a function of the color of the attended stimulus that the monkeys acted upon. High and low reward magnitude was 0.76ml and 0.4ml per successfully performed trial. High/low rewards were linked to the red/green color of the attended stimulus (with the color – reward mapping changing across blocks of 30 correctly performed trials). A key component of the task is that the location of covert spatial attention on one of the two colored stimuli (left or right periphery) is distinct from the possible locations to which the animal made a saccade (up- and downwards) to indicate the transient rotation of the attended stimulus.

2.3 - Anatomical reconstruction

The anatomical site of each recorded LFP was reconstructed for each monkey and projected onto the 2D flat map representation of a standardized macaque brain ('F99') available within the MR software Caret (Kaping et al., 2011). **Fig. A1** survey's the main procedure for two example reconstructions. Reconstruction began by projecting each electrodes trajectory onto the two dimensional brain slices obtained from 7T anatomical MRI images, using the open-source OsiriX Imaging software and custom-written MATLAB programs (The Mathworks Inc.), utilizing the iodine visualized electrode trajectory within the electrode grid placed within the recording chamber during MR scanning. The coronal outline of the cortical folding of the MR

gray scale image was drawn to ease the comparison of the individual monkey brain slices to standard anatomical atlases, before projecting the electrode tip position into the standardized macaque brain (F99) available in Caret. Note that the individual monkey brains were initially reproduced within the Caret software to validate similarity and derive the scaling factors to match the lower resolution monkey MRs to the higher resolution standard F99 brain. The electrode position was manually projected, under visual guidance, to the matched location in the standard brain in Caret. In the MATLAB scripts, anteroposterior angle of the electrode trajectory (the four chambers in the two animals had anteroposterior angles of 0º, 0º, 5º, and 10º, respectively) was adjusted so that the projected 3D electrode tip position was the actual position of the tip in the correct coronal place

After identifying all recording sites within the standard brain, Caret software was used to render the sliced brain into a 3-dimensional volume, spherically inflated and cut it to unfold the brain into 2-dimensional space (**Fig. 2B** and **Fig. A1**). In an independent procedure, the major anatomical subdivision schemes of the fronto-cingulate cortex was visualized using the labeling scheme from Barbas and Zikopoulos reference ((Barbas and Zikopoulos, 2007); *see* **Fig. A1C**). Two other prefrontal / cingulate cortex subdivision schemes that are used in the literature were visualized in in the same 2-D flat map in **Fig. A1D** to allow comparison with the Barbas & Zikopoulus scheme of the cortical fields (for details, *see* (Kaping et al., 2011)). These alternate subdivision schemes are highly similar to the schema that was used for assigning cells to anatomically defined brain areas.

2.4 - Definition of error trials

Error trials were defined as those where the monkey either made an error in discriminating the transient rotation of the target, or responded during the 600 ms following a

rotation event in the distractor stimulus. Thus, all errors were committed after a stimulus change (rotation) happened (*see* Shen et al., 2014).

2.5 - Analysis of cross-frequency phase-amplitude correlations

I analyzed how phase variations of low frequency oscillations relate to variations of amplitude in high frequency oscillations.. Following methodological guidelines proposed by Aru and colleagues (2015), I consider this phase-amplitude (P-A) cross frequency analysis to reflect P-A correlations instead of the more common label P-A coupling, as our experiment does not include direct manipulations for testing whether there are direct interactions of activity across different frequencies (Aru et al., 2015).

All main analysis steps and statistical routines described in the following are available publicly online under a GNU license at http://attentionlab.ca/doku.php?id=analysis-tutorials.

I hypothesized that cross frequency correlations subserves attentional selection. As a first step, raw LFP signals were bandpass filtered with a 4th order, two pass Butterworth filter and subsequently Hilbert transformed. I employed a variable bandpass filter defined as ±⅓ of the centre frequency (e.g. 7±2.3Hz as [4.7 9.3] Hz, or 40±13.3Hz as [26.7 53.3] Hz), which has been shown to improve detection of cross frequency interactions (Aru et al., 2015). I quantified P-A correlation between low frequencies in the range of 4-29 Hz (with 1.5 Hz steps) and high frequencies in the 30-130 Hz range (with 3 Hz steps). I selected channel combinations where the phase and amplitude channels are recorded from different electrodes to avoid spurious coupling as a result of a non-stationary input (Aru et al., 2015). I quantified cross frequency correlation between the low frequency (f_p) phase of the analytic signal $x_{fp}(t)$ and the high frequency (f_a) amplitude of the analytic signal $x_{fa}(t)$ using Tort's MI (Tort et al., 2010) and Maris' wPLF (van der Meij et al., 2012). These signals were derived by concatenating, for a single channel, all

recorded trials into one signal. I analyzed and compared oscillatory activity in two 500 ms epochs, just before and just after attention cue onset. The procedures are summarized here.

2.6 - Analysis of cross-frequency interactions using Tort's Modulation Index.

The MI is based on the Kullbeck-Leiber distance between two empirical distributions, and is closely related to Shannon entropy. In calculating the MI, the phases of signal $x_{fp}(t)$ are extracted and binned (N=18 bins, *see* (Tort et al., 2010)). The mean amplitude $\mathbf{M(j)_{mean}}$ of $x_{fa}(t)$ is then calculated over each phase bin ***j***. Finally, each $\mathbf{M(j)_{mean}}$ bin is normalized by the mean of all $\mathbf{M_{mean}}$, yielding the distribution **P(j)**.

The null-hypothesis of the test is that the expected amplitude-distribution is uniform. The Kullbeck-Leiber distance (D) is:

$$D(P,Q)=\sum_{j=1}^{N} P(j)\cdot\log\left(\frac{P(j)}{Q(j)}\right) \qquad \textbf{Equation 1}$$

where distribution **P** is the observed amplitude distribution, distribution **Q** is the uniform distribution, and **N** is the number of samples. The MI is the normalized Kullbeck-Leiber distance:

$$MI=\frac{D(P,Q)}{\log(N)} \qquad \textbf{Equation 2}$$

2.7 - Analysis of cross-frequency interactions using the weighted Phase Locking Factor

The weighted Phase Locking Factor (wPLF) is an inner-product of the complex signals $x_{fp}(t)$ and $x_{fa}(t)$ (van der Meij et al., 2012). Its magnitude indexes the strength of P-A correlation, while its phase indexes the preferred phase of high frequency activity (van der Meij et al., 2012).

Each signal is mean centred (mean amplitude over the signal subtracted from each entry) and normalized by dividing by the signals' norm. The magnitude of the derived high frequency signal ***A(t)*** is taken, resulting in a real-valued signal, while the low-frequency ***P(t)*** derived signal remains complex valued. The wPLF is then:

$$wPLF = \langle A(t), P(t) \rangle \qquad \textbf{Equation 3}$$

2.8 - Testing for changes in cross frequency correlation.

Across the population of LFP-LFP recording pairs, I compared cross frequency correlation in the 500 ms before attention cue onset ('pre-cue') to the 500 ms in the post attention cue period ('post-cue') (see **Fig. 2** and **Figure A3**). The pairwise difference in P-A correlation was normalized such that:

$$\Delta CFC = \frac{CFC_{post} - CFC_{pre}}{CFC_{post} + CFC_{pre}} \qquad \textbf{Equation 4}$$

where *CFC* is the cross frequency correlation as measured using the MI or wPLF (see above).

WeI tested the significance of the change in P-A correlation across the population of LFPs by applying a Wilcoxon sign-rank test for each phase-to-amplitude frequency combination (α=0.05), corrected for the false discovery rate (FDR) using the Bonferroni-Holm's method. Analysis was performed separately for correct and error trials.

2.9 - Statistical surrogate analysis of single LFP-pair cross-frequency correlation

I further analyzed cross frequency correlation by selecting LFP pairs that showed a significant change in P-A correlation, as determined by a surrogate shuffling method. To this end, a surrogate high-frequency signal was derived by offsetting $x_{fa}(t)$ by a random, large amount

(in other words, by splicing the signal in two). This procedure was repeated 200 times, which allowed the derivation of a p-value. Because the wPLF has the potential to be biased by power in the low-frequency band, I used the MI to select significant channels. All subsequent analysis (regarding preferred phase and anatomical specificity) was conducted on those LFP pairs that individually showed a significant increase in P-A correlation.

2.10 - Temporal specificity of theta-gamma phase-amplitude correlation

I determined the time of maximal (peak) P-A correlation by calculating the MI in 500 ms windows analyzed every 100 ms, first in the 500 ms pre-cue period and subsequently every 100 ms from 0 ms to 1000 ms (seven windows total; see **Fig. 3E**). MI values were masked to a value of zero if they did not achieve statistical significance, and averaged in the LFPs in the P-A correlated frequencies of interest determined earlier.

2.11 - Controlling for differences in trial number between correct and error trials

On average, there were fewer error trials than correct trials. To control for a bias related to the different number of trials, I used a shuffling procedure whereby for each LFP pair identified above, I selected at random the same number of correct trials as there were error trials. This procedure was repeated 1000 times, from which I built a distribution of shuffled MI values. I then compared the observed difference in MI on error trials (**equation 4**) with the distribution of shuffled MI difference values from correct trials for the pair of P-A correlated frequencies identified in the previous analysis. I also tested whether the MI across different LFP pairs was higher on each distribution of error-matched correct trials vs error trials (Wilcoxon sign-rank test, 1000 surrogates).

2.12 - Analysis of the low frequency phases of gamma frequency correlation

The MI allowed determining the preferred phase by finding the circular average of the phase bins, weighted by the amplitude probability in each phase bin. Circular statistics were performed using the CircStats toolbox (Berens, 2009). I determined the circular distribution of the mean preferred phases of the LFPs channels with significant theta-gamma P-A correlation for both correct and error trials, and used the non-parametric Hodjes-Ajne test to determine if these distributions differed significantly from a uniform angular distribution. I also tested whether two distributions differed from one another via the Kuiper test. Both of these tests do not assume a von Mises distribution.

If there would exist multiple preferred coupling phases, the MI amplitude distribution would be multi-modal. In such a case, it may be that the mean preferred phase is in fact a trough between peaks of the amplitude distribution. To control for the effects of multi-modality, I extracted preferred phases by finding the mean phase of peaks in the amplitude distribution. A bin was considered a peak if it was higher than a set threshold of the difference between the global maximum and minimum of the amplitude distribution (threshold =100, 80, 70, 50 %). I assessed uniformity using the Hodjes-Ajne test, and similarity between distributions using the Kuiper test.

I repeated the analysis of preferred phase of the amplitude distribution after equalizing the number of correct trials to that of error trials. Multiple surrogates were thus created. For each LFP pair, I took the circular average of phases across surrogates. Where the number of correct trials was less than the number of error trials, I used the observed preferred phase in lieu of the average across surrogates. All subsequent analysis (of the preferred phase, uniformity, and comparison to error trials) mirrored the analysis described above.

As mentioned previously, the phase of the wPLF is the mean preferred phase of high

frequency activity. I also determined the distribution of preferred phases and their similarity to the preferred phase distributions described above via the Hodjes-Ajne and Kuiper tests.

The summary of the results using different phase extraction methods is shown in **Table A1**.

2.13 - Anatomical specificity of theta-gamma phase amplitude correlation

I used adjacency matrices to visualize the anatomical specificity of theta-gamma P-A correlation (**Fig. 5A**,**B**). The x-axis (y-axis) corresponds to the areas where channels from which the low frequency phase information (high frequency amplitude information) were derived. Because there are a different number of recorded channels in each area, I report on the proportion of channels exhibiting theta-gamma P-A correlation for each area combination using statistical analyses outlined by (Zar, 2010).

I assessed whether the global distribution of P-A correlated channels was independent of anatomical recording location via a χ^2 test on a 3x3x2 contingency table crossing location of phase LFPs with location of amplitude LFPs with the LFP pairs' status of coupling (i.e. was significant theta-gamma correlation found?; *see* **Fig 4**). I used a Z-score with a Yates correction for continuity for each individual area pair. Z-scores were assessed at a significance of $\alpha=0.05$ (corresponding to a Z-score of 1.96).

I also asked whether a particular subarea within the ACC/PFC was more likely to contribute phase or amplitude information for the inter-areal P-A correlations. To this end, I counted the number **N(t,a)** of all channels where either the phase or amplitude channel came from a particular area:

$$N(t,a)=\sum_{i}^{n}\sum_{j}^{n} m_{i,j} \qquad \textbf{Equation 5}$$

where **N** is the number of type **t ={amplitude, phase}** channels found in area **a ={1,…,n}** during theta-gamma P-A correlation, and **n** is the number of areas. The matrix **m** is an adjacency matrix indexing the number of LFP pairs per area combination (as described above). When considering either phase or amplitude channels, **i** or **j** remains constant, respectively, and is equal to **a**. In other words, I sum across a column or row of matrix **m,** depending on whether we're concerned with phase or amplitude providing LFPs. Since I considered only inter-areal P-A correlation in this analysis, I ignored entries where i=j=a. Finally, the likelihood **P(t,a)** that a particular area is more likely to contribute phase or amplitude information during inter-areal P-A correlation is:

$$P(t,a)=\frac{N_{couple}(t,a)}{N_{all}(t,a)} \qquad \textbf{Equation 6}$$

where the subscript 'couple' refers to LFP pairs that exhibited significant P-A correlation, and "all" refers to all recorded LFP pairs (**Fig. 5D**).

As a first step, I determined if the distribution of phase or amplitude channels across all recorded areas is significantly different than expected using a χ^2 test. Secondly, I asked whether the difference in the proportion of the observed amplitude or phase channels was significant for a particular area. Because channels in an area are not independent, I used the Mcnemar test on a 2x2 contingency table, crossing the kind of information the LFP contributed during theta-gamma P-A correlation (i.e. did the LFP contribute phase information, yes/no? amplitude information, yes/no?). I performed the test using the **mcnemar.m** function provided by Cardillo 2007 at http://www.mathworks.com/matlabcentral/fileexchange/15472. Finally, I assessed whether the individual observed frequencies of amplitude or phase information donation during P-A

correlation across all recorded areas was different than expected by chance using a Z-score test.

2.14 - Relation of maximal gamma amplitude to cue-onset time and low frequency phase

I compared the variability (i.e. jitter) of the peak in the gamma envelope relative to the cue onset time and relative to the phase of the theta frequency band (Aru et al., 2015). I extracted the peak in the gamma (40 Hz-filtered) amplitude envelope, and recorded the time from cue onset as well as the concurrent phase in the theta frequency signal. I then computed the variance of the time, and the circular variance of the phase. The phase variance was converted to milliseconds, which allowed a direct comparison between the time and phase.

2.15 - Relation of phase amplitude correlation to changes in LFP power

I assessed if the P-A theta gamma correlation that was identified was related to LFP power. To this end, I first calculated the power by squaring the amplitude envelope (derived from the Hilbert transform), and summing in the epoch of interest. I correlated power in low and high frequency ranges with the MI from LFP channels showing P-A correlations using the Spearman rank correlation.

2.16 - Relation of phase amplitude correlation to theta phase

I assessed the phase consistency across trials for unique channels from which the theta signal (and subsequent phase data) was taken. For each channel, the instantaneous mean angle of either correct or error trials was determined using the **circ_mean** function across trials (Berens, 2009) Statistical significance of phase consistency was determined by taking the instantaneous Rayleigh Z score and associated p-value using the **circ_rtest** function (Berens, 2009). This data was used to assess the temporal latency of maximal phase consistency. First, I determined the

proportion of phase channels that showed a significant Rayleigh Z score for each point in time (**Fig. 6B**, *left panel*). Second, I divided the -500 ms to 500 ms time resolved Rayleigh's Z data into ten equally spaced time bins. For each phase channel, I recorded the time in which the peak Rayleigh Z value occurred (**Fig. 6B**, *right panel*). In this way, I generated a proportion of channels that peak within a particular time bin, allowing us to perform a χ^2 test to determine if the distribution of Rayleigh Z peaks in time is significantly different from the null hypothesis that the distribution is uniform. Finally, I determined which phase channels showed phase consistency 100-300 ms post-cue (as determined from the prior analysis) at $p<0.05$ in order to locate them on the cortical sheet (**Fig. 6C**).

2.17 - Relation of phase amplitude correlation to the average field potential

I determined the average LFP potential aligned to the attention cue onset using the fieldtrip function **ft_timelockanalysis** on correct trials and on error trials separately for all phase or amplitude providing LFPs. The average field potential was plotted in relation to the cue-onset time.

I then used the behavioral outcome as a way to dissociate the influence of the average field potential on attention processing, using cluster level analysis reviewed by Maris and Oostenveld (Maris and Oostenveld, 2007). Briefly, a time-resolved t-test was performed across average cue-aligned field potentials for individual phase-or amplitude- LFPs between correct and error trials. I then determined temporal clusters of interest by summing the t-value for adjacent time points with a similar sign that showed a significant ($p<0.05$) difference. Statistical reliability was determined by a Monte Carlo surrogate test. Average field potentials of different phase- or amplitude- channels associated with either correct or error trials were shuffled, and then surrogate correct and error sets were reconstructed by randomly sampling from the pool, and the

cluster statistic recalculated. A cluster was deemed significant if its value was greater than 95% of permuted clusters (i.e. $p<0.05$). The analysis was run on a temporal window spanning -700 ms to +500 ms (aligned to attention cue onset), as determined by a visual inspection of the average field potential.

2.18 - Relation of phase amplitude correlation to LFP phase synchronization

I next determined the degree of phase synchronization across theta-gamma phase amplitude correlated LFPs, and whether they were related to either the degree of P-A correlation or to the cue-triggered LFP phase reset. I determined phase synchronization with the *debiased* weighted phase lag index (wPLI; *see* (Phillips et al., 2013)) using functions from the FieldTrip toolbox (Oostenveld et al., 2011). Note that this is not related to the 'weighted phase locking factor' described above. This measure is insensitive to noise and volume-conduction effects, and also corrects for the positive bias the wPLI has for small sample size. I will refer to the debiased wPLI as the wPLI in this text.

I calculated the wPLI for both correct (**Fig. A6A**) and error trials (**Fig. A6B**) in the 85 theta-gamma phase amplitude correlation channels where there was a significant increase in coupling detected via the MI. To compare them to the MI values I obtained, I restricted wPLI time of interest to the 500 ms before and after attention cue onset.

I determined, independently for each behavioural outcome and temporal epoch, whether the wPLI was significantly different from 0 with Wilcoxon sign rank test. To determine if there was a change in wPLI after attention cue onset, I used a Wilcoxon sign rank test for paired samples. Tests were significant if $p<0.05$, after Bonferroni-Holm's correction for the FDR.

To compare the phase synchronization to phase amplitude correlation, I restricted further phase synchrony analysis to the same frequency range as determined by the phase amplitude

correlation analysis. I tested for a difference in wPLI across behavioural outcomes with a Wilcoxon signed rank test for paired samples, independently for the pre- and post-cue epoch. I also correlated the MI with the wPLI using Spearman rank correlation. Finally, to draw a link between the phase resetting LFPs and phase coupling, I correlated the wPLI in the pre-cue with the post-cue epochs, and then highlighted those data points where the phase-donating LFP showed a significant phase reset in the 100-300 ms post cue (**Fig. A6C**).

2.19 - Dissociating value and spatial information contribution to theta-gamma phase-amplitude correlation

Cross-frequency correlation may be selective for ipsi- or contralateral shifts of attention. By the same token, shifting attention to a target stimulus with a higher or lower associated reward may influence the strength of theta-gamma cross-frequency correlation. I thus tested whether I could find evidence whether cross-frequency correlation shows spatial selectivity or selectivity for the relative reward magnitude associated with targets.

As a first step, I calculated the normalized change in theta-gamma P-A correlation (quantified using the MI, **equation 4**) from pre- to post- attention cue separately for contra vs ipsi-lateral conditions, or high vs low rewarded targets. I tested whether the average change in theta-gamma P-A correlation change across all LFP pairs could dissociate between two separate attention conditions via a Wilcoxon sign-rank test. This was performed across the entire population of LFP pairs, and across those n=85 LFP pairs that showed individually significant increases in theta-gamma P-A correlation (unless stated otherwise).

As a second analysis approach I tested whether theta-gamma P-A correlation of individual LFP pairs is selective for attention conditions. I assessed this via a Monte Carlo surrogate test. First, the change in theta-gamma P-A correlation as indexed using the MI (dMI,

equation 4) was calculated for two attention conditions separately (e.g. dMI_{contra} vs dMI_{ips}). Next I calculated the difference across the conditions. For spatial conditions, I used:

$$D_{spatial}=dMI_{contra} - dMI_{ips} \quad \textbf{Equation 7}$$

While for value conditions I used:

$$D_{reward}=dMI_{high} - dMI_{low} \quad \textbf{Equation 8}$$

For example, positive value of $D_{spatial}$ (> 0) indexes a relative increase in theta-gamma correlation when the cue shifts attention contralaterally, while negative (< 0) values reflect a relative increase in theta-gamma correlation with attention ipsilateral to the recording site.

To assess significance, I shuffled the trial labels, and recalculated D'.
This procedure was repeated 200 times, and the observed D was compared against the distribution of D'. Finally, I determined if LFP pairs informative of correct attentional deployment overlapped with LFP pair informative of ipsi- or contralateral attention, or of high vs low reward magnitude. I determined LFP pairs that individually differentiated between two conditions via the change in MI in the previous analysis, and compared these to those comprising the functional network analyzed in the main text.

2.20 - Quantifying attention information in the firing rate of recorded neurons

Firing rate at LFP sites engaged in cross-frequency correlation may be different from those sites that are not thus engaged. To test for this possibility, I extracted the firing rate of neurons from those electrodes that provided either LFP phase or LFP amplitude information in the theta-gamma phase amplitude correlation analysis. I tested for a difference between firing rate in the post-cue epoch in the theta-gamma paired sites and all others via a Wilcoxon rank test.

Likewise, I used the same test but on the change in firing rate after cue onset as compared to before onset. I determined if there was a more subtle relationship between absolute MI and firing rate, or the change in MI and firing rate, by computing Spearman R correlations.

I quantified attention selective modulation of firing by computing the normalized difference in firing when attention shifted contra- versus ipsi- lateral:

$$AI_{rate} = \frac{firing_{contra} - firing_{ips}}{firing_{contra} + firing_{ips}} \qquad \textbf{Equation 9}$$

The AI_{rate} is positive when firing was larger with contra- than ipsi- lateral attention shifts, and negative when the firing was larger for ipsilateral attention trials. I quantified attention modulation in theta-gamma correlation in the same way as the firing rate by indexing the strength of theta-gamma correlation during contra- versus ipsilateral attention shift in the same 500 ms post-cue time window as the firing rate modulation. Additionally, I also quantified spatially specific *changes* in theta-gamma correlation as I have done in the main analysis. I thus calculated the change from theta-gamma correlation form the pre-cue interval to the post-cue interval separately for the condition when the cue indicated a contralateral or an ipsilateral shift **(equation 4)**. I then contrasted this attention cue specific change in theta-gamma correlation between attention conditions (**equation 7**).

2.21 - Comparison of theta-gamma correlation of LFP-LFP pairs with the strength of burst-LFP synchronization

I tested whether the strength of theta-gamma LFP-LFP correlation is related to the strength of burst-LFP synchronization following procedures outlined in (Womelsdorf et al., 2014a) and described in brief below. To test for this I performed the following analyses steps.

First, I selected for analysis those single isolated neurons that showed within either 500

ms before or 500 ms after the attention cue onset at least n=30 burst spike events across all trials where monkeys shifted attention either contra- or ipsi-laterally. Burst spike event were defined as before as spike successions with ≤5ms interspike intervals. Spike recording techniques are described in detail in (Womelsdorf et al., 2014a).

Second, I calculated burst-LFP synchronization for all electrode combinations at which I recorded LFPs for the theta-gamma phase amplitude correlation analysis. Analysis was restricted to burst - LFP recording pairs from different (spatially distant) recording sites. To quantify the strength of burst-LFP synchronization I followed the procedure described in detail in (Womelsdorf et al., 2014a). In brief, I selected for all burst events the first spike of the burst and calculated how phase consistent these burst spikes were to the LFP at the three frequencies described above (theta: 5-10 Hz, low-β: 10-20 Hz, mid-gamma 55-75 Hz). LFP phases were obtained by Hanning-tapered Fast Fourier transforms of the LFP in a time window ±250 ms around the time of the first burst spike. I indexed the synchronization of burst spikes to the phase of theta/low-β/mid-gamma frequencies using the pairwise phase consistency which is a measure that is unbiased with regard to the number of observations (i.e. not biased by the number of spike events; *see* (Womelsdorf et al., 2010)).

Third, I sorted the burst-LFP pairs into different conditions based on whether the electrode providing the burst firing neurons was the same as the theta LFP phase providing channel, or the gamma amplitude providing channel, or whether the LFP channel that was paired with the burst firing neuron channel was the same as the theta- or gamma- providing channel (see Table 1 for the complete matrix of conditions). For each condition I then obtained the Spearman rank correlation coefficients between burst-LFP synchronization and theta-gamma LFP-LFP correlation, which I report in **Table S2**.

CHAPTER 3: PHASE AMPLITUDE CORRELATION IN THE ACC & PFC

I analyzed LFP activity from 1104 between-channel pairs of electrodes (344 individual LFP channels) within different subfields in ACC/PFC of two macaques engaged in an attention task (**Fig. 2A**). In the following, I report results pooled across monkeys and show that individual monkey results were consistent and qualitatively similar in **Result A1.** These recordings were from a dataset that was previously analyzed with respect to neuronal firing and burst LFP synchronization ((Kaping et al., 2011; Womelsdorf et al., 2014a; Ardid et al., 2015); *see* **Methods**). During each trial, covert spatial attention had to be shifted towards one of two peripheral stimuli in response to the color of a centrally presented cue stimulus (**Fig. 2A**). Covert spatial attention then had to be sustained on the target stimulus until it transiently rotated clockwise or counterclockwise. The animals obtained fluid reward when they correctly discriminated the rotation of the attended stimulus. On half of the trials, the distracting non-target stimulus rotated before the target stimulus. Both monkeys successfully ignored this distractor change indicating correct attentional deployment on the target with an average accuracy of 82.6% ± 0.7 SE and errors committed in response to the distractor rotation in 4.5 ± 0.2% SE)(see **Result A2**).

3.1 - Attention cue triggers theta-gamma phase-amplitude correlations.

In the outlined task, attention shifts required the use of task knowledge to successfully combine color and location information to prioritize the correct stimulus. ACC/PFC subfields are core circuits supporting the flexible integration of information to shift attention (Kaping et al., 2011; Shenhav et al., 2013). To test whether the attention shift is accompanied by cross-

frequency interactions, LFP pairs recorded from *different* sites in ACC and PFC were analyzed (**Fig. 2B**, and **A1 Figs. S1, S2**) and quantified how high frequency activity variations related to the phases of slow frequency activity modulation around the time of the attention cue. In multiple example LFP pairs, the attention cue onset triggered sequences of brief bursts of gamma band activity that synchronized to a narrow phase range of periodic 5-10 Hz theta band activity recorded at distant sites (**Fig. 2C, Fig. A2**). To quantify whether these cross-frequency correlations were reliably linked to attention shifts, I calculated the change in Tort's modulation index (Tort et al., 2010) in 500 ms time windows following the attention cue versus before the cue. Across all between-channel LFP pairs, there was a significant increase in cross-frequency correlations between the phase of a ~7 Hz theta frequency, and the amplitude of ~40 Hz gamma frequency activity (Wilcoxon sign-rank test, $p=1.6*10^{-4}$, FDR corrected; **Fig. 3A**, **B; Fig. A3**). Across all LFP pairs, the theta-gamma phase-amplitude (P-A) correlations increased on average by 61.73 ± 0.037 % SE (average normalized change in MI: 0.0556 ± 0.0109 SE, **Fig. 3B**). For the 7-to-40 Hz theta-gamma frequency combination that showed maximal correlation, n=85 LFP pairs (85/1104 = 7.7%) showed a statistically significant increase in P-A correlation following the attention-cue (Monte Carlo surrogate test, at least $p < 0.05$; **Fig. 3B**). In the following I characterize these 85 LFP pairs that showed an increased theta-gamma correlation in the post-cue period that was also evident in the average across the population of LFP pairs (see **Result A3** for a characterization of n=46 (4.2 %) LFP pairs showing significant reductions in theta-gamma correlation in the post cue epoch). Theta-gamma correlation of these 85 LFP pairs was based on 74/344 (21.5%) LFP channels contributing theta-phases, and 67/344 (19.5%) LFPs contributing gamma-amplitude variations. Overall, 122/344 (35.5%) unique LFPs contributed to LFP pairs with theta-gamma correlation that was significant and consistently evident in both monkeys

(**Result A1.1**). Observing reliable theta-gamma correlation was not dependent on the metric used to measure P-A correlation, as results were essentially identical when applying the weighted phase locking factor ((van der Meij et al., 2012); **Fig. A4**). Consistent with this finding, 73% of those LFPs that provided the theta phase for significantly phase-amplitude correlated pairs also showed an apparent theta-band peak in the power spectra (**Fig.'s A5, A6**). Power modulations at theta did not, however, correlate with cue triggered increases of theta-gamma correlations (see **Result A4**).

I next tested whether the LFP gamma amplitude variations were statistically more precisely locked to the theta phases of LFPs or to the cue onset. If the latter were the case, then theta-gamma correlations could be secondary to cue-triggered gamma amplitude changes (Aru et al., 2015). However, on average across the n=85 LFP pairs with significant theta-gamma correlations that the maximum gamma amplitudes showed less variance in the phase of their theta band modulation than in their time to attention cue onset (**Result A5; Fig. A3C**).

3.2 - Theta-gamma correlations fail to emerge on error trials.

Theta-gamma P-A correlations could accompany attention cues irrespective of whether attention shifted correctly, which would render the phenomenon functionally unimportant to attentional control. I thus compared correctly performed trials to error trials, where subjects either responded to the distractor (indicating either wrong attention shifts or low attentional control levels) or made erroneous choices during the time the target should have been selected (indicating e.g. failed perceptual discrimination of the attended stimulus likely also related to low attentional control levels (Shenhav et al., 2013; Shen et al., 2014). In contrast to correct trials, the attention cue did not trigger a significant increase in phase-amplitude correlation on error trials (Wilcoxon sign-rank test, p=1, FDR corrected; **Fig. 3C**). The lack of P-A correlation was evident

across the whole population of LFP pairs as well as for the subset of LFP pairs that showed individually significant P-A correlation on correct trials (**Fig. 3D**). This effect is readily visible in the average MI comodulograms (**Fig. 3E**), and remained robust when equalizing the number of correct trials to the lower number of error trials (**Result A6**). Testing the temporal specificity of this error predicting effect across all LFP pairs showed that theta-gamma correlations were maximal on correct trials immediately following cue onset, but remained higher than chance levels, and higher than on error trials, over the entire post-cue analysis period (up to 0.75 sec. ±0.25) (**Fig. 3F**).

The lack of P-A correlations on error trials may follow from a larger variability of theta phases at which gamma activity synchronizes, from a systematic shift in theta frequency locked phases, or a combination of both (Onslow et al., 2014). To elucidate these possibilities I characterized the theta phase at which gamma activity modulations aligned on correct and on error trials (**Fig. 4**). Across LFP pairs with significant theta-gamma correlation, gamma bursts on correct trials phase locked on average close to the peak of the theta cycle after the attention cue (mean phase of -14.69^0, 95% CI [-41.01^0, 11.63^0]), with a significantly nonuniform circular phase distribution (Hodjes-Ajne test, $p=3.6*10^{-4}$; **Fig. 4A**). In contrast, the distribution of phases on error trials only revealed a statistical trend to deviate from uniformity (Hodjes-Ajne test, $p=0.064$), with a mean phase that was about 90^0 offset from the mean phase on correct trials (-94.28^0, 95% CI [-131.40^0, -57.16^0]; **Fig. 4B**). Importantly, correct and error trial phase distributions were significantly different (Kuiper test, $p<0.005$), suggesting that on error trials, theta phases shifted and showed a larger variability compared to correct trials (**Fig. 4C;** *see* **Result A1.2** for consistent effect across monkeys). Control analyses revealed the same functional effects when accounting for the lower overall modulation strength on error trials compared to

correct trials (**Result A7, Table 1**), as well as for the differences in trial numbers (**Result A6**). Moreover, the average field potential of the LFP around the attention cue onset did not distinguish correct from error trials, suggesting that possible non-stationary transients do not account for the functionally significant P-A correlations (*see* (Aru et al., 2015), **Result A8**).

3.3 - Inter-areal cross-frequency correlation is anatomically specific.

I next asked whether the anatomical location of the theta phase and gamma amplitude providing LFPs in ACC/PFC mattered for P-A correlations. One assumption of this analysis is that theta-phase providing sites may more likely serve as modulating sources for attention, while gamma-amplitude providing sites relate to implementing attention. To test this, I reconstructed the LFP recording locations (*see* **Fig. A1**) and grouped them into the ventromedial PFC (areas 32 and 10), ACC (area 24) and lateral PFC (areas 46, 8 and 9) (**Fig. 5A**). Among the significantly theta-gamma correlated pairs, phase and amplitude providing LFPs were found in each of the subareas, but with an apparent asymmetry between areas (**Fig. 5B,C;** *see* **Result A9 and A1.3**). Testing each area for whether they contained more phase or amplitude LFPs, the lateral PFC theta-phases were significantly less likely to correlate with ACC gamma-amplitudes (Z-test, p=0.0089; **Fig. 5C**). More specific testing of the inter-areal P-A correlations showed that the lateral PFC had overall less inter-areal theta-phase providing LFPs than expected by chance (Z-test, p=0.029; **Fig. 5D**), while the ACC had less inter-areal amplitude providing LFPs (Z-test, p=0.028; **Fig. 5D**). Consistent with this finding, the ACC provided overall significantly more theta-phase LFPs than gamma-amplitude LFPs during inter-areal theta-gamma correlations (McNemar χ^2 test, p=0.034; **Fig. 5D**), while the LPFC showed a trend for more amplitude than phase providing LFPs (McNemar χ^2 test, p=0.066; **Fig. 5D**). These results were similar in both monkeys (**Result A1.3**).

3.4 - Cue induced theta-phase reset in LFPs showing theta-gamma correlation.

Theoretical studies suggest that the modulation of low frequency phase is instrumental in triggering high frequency bursts during theta-gamma correlations (17, 18). Such precedence of low frequency activity for P-A correlation would empirically become evident as a re-alignment, or reset, of phases (Van Atteveldt et al., 2014). I tested for the presence of an attention-cue triggered theta-phase reset and its putative relation to theta-gamma correlation, and found that immediately following the attention cue the average theta band phases became highly similar across individual LFPs that showed significant theta-gamma correlations. This phase alignment was visually apparent on correct trials but not on error trials (**Fig. 6A**). To quantify this phase reset, I calculated the significance of the instantaneous theta-phase consistency across trials for each LFP around attention cue onset and found that the greatest number of LFP channels exhibiting significant theta-phase consistency 268 ms after attention cue onset (**Fig. 6B**). The rise in theta phase consistent LFPs was evident on correct trials and failed to emerge on error trials. To validate this finding, I extracted the time at which the Rayleigh Z time course peaked in the 1000 ms around the time of the attention cue onset for each LFP. Corroborating the previous result, 41.89 % of the theta phase-providing LFP sites (31/74) showed *peak* phase consistency 150-250 ms (± 50 ms) after attention cue onset on correct trials (**Fig. 6B**). This distribution of peak phase consistency was significantly non-uniform on correct trials, but not on error trials (Pearson's χ^2 test, p=0.0012 and p=0.465, respectively). In the 150-250 ms (± 50 ms) time window, 35/74 phase-providing LFP sites showed a significant theta band phase consistency, and clustered at the nexus of the ACC, VMPFC and lateral PFC (**Fig. 6C**).

The presence of a theta-phase reset could synchronize LFP theta phases across multiple ACC/PFC subfields. Thus, the correlation of gamma amplitudes to theta phases could be

understood as a direct consequence of such large-scale theta-band coherence. However, LFP-LFP theta-phase synchronization did not change from pre- to post- attention cue, was not different between correct and error trials, and did not correlate with the increase of inter-areal theta-gamma correlation during attention shifts (**Result A10**).

3.5 - Selective theta-gamma correlation for target locations and reward value, and its relation to firing rate information.

Theta-gamma correlation may not only emerge selectively on correct versus erroneous attention shifts, but may carry specific task-relevant information about the direction of the attention shift. Across the entire population of LFP pairs, there was a statistical trend for larger theta-gamma correlation when attention shifted to the contralateral versus ipsilateral stimulus (Wilcoxon sign rank test, $p=0.066$; **Figure S7A, Result A11.1**). Testing for significant differences in theta-gamma correlation between spatial conditions at the single LFP pair level revealed that a small subset of LFP pairs (4.4%=49/1104) showed significant effects (Monte Carlo surrogate test, two-sided, $p<0.05$), with n=32 (n=17) LFP pairs showing larger theta-gamma correlations for contralateral (ipsilateral) attention shifts (see **Result A11.1**). In addition to spatial attention, I tested in a subset of sessions whether theta-gamma correlations emerged differentially when the cue directed attention to a target stimulus with higher versus lower reward association, but did not find consistent differences of theta-gamma correlations for higher or lower rewarded attention targets (**Result A11.2**). LFP pairs where theta-gamma correlations for dissociated locations or rewards were largely unrelated to LFP pairs with theta-gamma correlations predictive of correct choices (**Figure S7B**, **Result A11.1, 11.2)**

CHAPTER 4: THETA-GAMMA CORRELATION & SINGLE UNIT EVENTS

In rodents, studies showing that theta-gamma correlation is instrumental to neural processing also show modulation of single neuron activity in relation to theta and gamma LFP oscillations (Huxter et al., 2008; Sirota et al., 2008; Lisman and Jensen, 2013). Often, as in the phase precession example described in the introduction, single units are active at specific phases of theta and gamma cycles, suggesting tight temporal ordering of single unit activity. Previous work on this dataset has shown that information about the spatial location and reward value of the target is represented in the firing rate, and is anatomically clustered across the PFC and ACC (Kaping et al., 2011). A separate analysis found bursts synchronizing to distal theta, beta, and high-gamma (Womelsdorf et al., 2014a). In the following analysis, we determined the relationship between theta-gamma correlation analyzed thus far, with firing rate and burst events.

4.1 - The relation of theta-gamma correlations and firing rate modulation during attention shifts

In previously analyses of the same ACC/PFC dataset, our lab has shown that neuronal spiking activity carries significant information about the target location to which attention is shifted (Kaping et al., 2011; *see also* Tremblay et al., 2014). A large proportion of neurons increased firing when attention was shifted to a contralateral stimulus while a slightly lower proportion of cells increased the firing when attention shifted ipsilaterally.

One possibility is that these firing rate modulations at single recording sites are linked to cross frequency correlations of the LFP at the same recording site. For example, if the theta phase of the LFP at a recording site couples with the gamma amplitude of a distant recording site

during the attention shift, then this LFP-phase providing site may also have single neurons with firing rate modulations about the direction of the attention shift. Similarly, if the LFP gamma amplitudes at one recording site couple to the phase of distant recording sites during the attention shift, then neurons at the gamma amplitude providing LFP site may also modulate their firing. In both these hypothetical scenarios, the overall strength of cross frequency correlation could relate to the information in firing rates about the spatial location of attention during the post-cue attention period.

We tested these scenarios by performing two broader analyses. First, we tested whether firing rate information (e.g. higher firing rate for attend-contralateral than for attend ipsilateral) is related to the *overall strength* of cross frequency correlation of the LFP recorded at the recording site as the neuronal firing rates were recorded. This analysis rests on the assumption that the overall strength of theta-gamma correlation could be important for firing rate increases and decreases.

Secondly, we tested whether actual differences in theta-gamma cross frequency correlations between attention conditions (e.g. the strength of P-A correlation during attend contralateral compared to attend ipsilateral) relate to actual differences in firing rate modulation in the attention conditions. This analysis is based on the assumption that recording sites with attention information about the direction of the attention shift in the firing rates (e.g. higher firing for contralateral shifts) may also be more likely LFPs to engage in inter-areal cross frequency correlation. For example, if neuron firing is stronger for contra-lateral attention shifts, then the LFP theta phase or the LFP gamma amplitudes may be also stronger for contralateral attention shifts.

In a final analysis, we quantified the relation of attentional modulation of theta-gamma correlation with attention to a higher versus lower rewarded target stimulus to the firing rate modulation in both conditions.

4.1.1 - Relation of overall theta-gamma cross frequency correlation with the degree of firing rate information

With regard to the first analysis we extracted the firing of neurons from those electrodes that provided either LFP phase or LFP amplitude for theta-gamma P-A correlation analysis. Firing rate information was quantified as the absolute z-normalized difference of neuronal firing when attention was shifted to a stimulus contralateral versus ipsilateral from the recorded hemisphere. We used for this analysis the same 500 ms time window after the attention cue onset in which theta-gamma correlations were calculated (*see* **A1 Methods** for details).

We found that firing rate information was not different for neurons recorded at recording sites that provided either the LFP phase or the LFP amplitude for significant theta-gamma correlation increases following the attention cue compared to recording sites that did not participate in significant theta-gamma correlation (Wilcoxon Rank test on the differences in firing rate information: $p = 0.22$ for the LFP phase channels, and $p = 0.44$ for the LFP amplitude channels. The average firing rate Z score for sites with significant theta-gamma correlation: LFP-phase channels: 1.12 ± 0.07 SE; for LFP-amplitude channels: 1.11 ± 0.07 SE; the average firing rate Z score for sites without theta-gamma correlation: LFP-phase channels: 1.26 ± 0.03 SE; LFP-amplitude channels showed identical results: 1.26 ± 0.03 SE). These results were consistent across monkeys with no significant effect when data from each monkey was tested separately (all p values ≥ 0.09).

We next repeated the previous analysis but considered not the absolute cross frequencies correlation in the post-cue epoch but whether the LFP site showed significant increases or decreases in P-A correlation from the pre-cue to the post-cue epoch. Similarly to the previous analysis, the firing rate information was not different for LFP phase or LFP amplitude channels that showed significantly increased MI compared to LFP channels that did not show significant cross frequency modulation (for LFP phase channels: Wilcoxon. Rank Sum test, $p = 0.33$. Average Z score for LFP phase channels with sign. P-A modulation = 1.16 ± 0.09 SE; for channels without P-A modulation = 1.24 ± 0.03 SE; For LFP amplitude channels, $p = 0.84$; average Z score for LFP phase channels with sign. P-A modulation = 1.16 ± 0.08 SE; for, channels without P-A modulation, 1.25 ± 0.03 SE). We repeated this analysis also for the subset of LFP channels that showed a significant decrease in cross frequency modulation following the attention cue. Similar to the previous analyses we found that the firing rate information was not different for neurons at recording sites showing significant decreased MI versus channels showing no significant MI modulation (Wilcoxon rank sum test, all $p>0.05$). All but one of these analyses provided results similar across monkeys with no significant effect when data from each monkey was tested separately. The exception was for LFP phase providing channels from monkey R. The firing rates of neurons at these channels carried on average significantly more spatial attention information than neurons at channels with LFPs that did not significantly change theta-gamma correlation (Wilcoxon rank sum test, $p = 0.009$, average Z score = 1.88, ± 0.197 SE).

To exclude the possibility that the previous analyses overlooked a more gradual or subtle relationship of a change in cross frequency correlation and firing rate information in the post-cue epoch, we calculated Spearman rank correlations of both variables. We found that firing rate

information was not significantly correlated with the change in MI from pre- to post-cue (for LFP phase providing channels: r=-0.012, p=0.72; LFP amplitude providing channels: r=-0.05, p=0.16). These results did not change when we removed datapoints that qualified as outliers (defined as values >3 STD from the mean). These results were consistent across monkeys with no significant correlations when data from each monkey was tested separately (p values for monkey's M: p = 0.86 and R: p = 0.73).

In summary, these results suggests that LFP recordings that engage in long-range theta-gamma correlations are not more likely than other recording sites to coincide with neuronal firing rate modulation about the spatial target location.

4.1.2 - Relation of spatially specific theta-gamma cross frequency correlation with spatially specific firing rate information.

The previous analyses were based on z-transformed firing rate differences between spatial attention conditions that were rectified and not sensitive to the sign of the modulation (i.e. enhanced firing for contralateral vs ipsilateral attention or vice-versa was not distinguished). In this second analysis, we considered the sign of the firing rate modulation. We quantified attentional modulation of firing by computing the normalized difference in firing when attention shifted contra- versus ipsi- lateral as attention index for firing rate (**equation 9**), and contrasted the change in theta-gamma correlation on contralateral vs ipsilateral conditions **(equation 7).**

We found similar results using other methods of contrasting phase-amplitude correlation between conditions (e.g. that contrasted only the post-cue epoch cross frequency correlation, as opposed to $D_{spatial}$).

We first tested whether attentional modulation of firing rates was associated with attentional modulation of cross frequency correlations. Spearman rank correlations of AI_{rate} and $D_{spatial}$ across all channels were significantly, positively correlation (r=0.07, p=0.0416), but it was of modest size and was only a statistical trend when outliers (values >3 times STD) were removed (r=0.06, p=0.056). Similarly, the correlation of AI_{rate} and $D_{spatial}$ were marginally positive and non-significant when testing the LFP/neuron channels separately in the lateral PFC, ACC, and VMPFC. The same null results (all $p > 0.05$) were obtained when the correlation was restricted to those recording channels at which the attentional firing rate modulation (AI_{rate}) was significant (at $p < 0.05$) based on a Wilcoxon rank sum tests.

In conclusion, there is no prominent association of spatially specific firing rate modulation and spatially specific cross-frequency P-A correlations, but rather modest positive correlations that only partly satisfy statistical trends ($p<0.1$).

4.1.3 - Relation of reward specific theta-gamma cross frequency correlation with reward specific firing rate information

In addition to the shift to a right versus left stimulus location, the cue also directed attention to a relatively higher versus relatively lower rewarded target stimulus in the majority of sessions (*see* Methods). While the reward magnitudes were not instrumental for performance (i.e. the animals had to perform the task irrespective of whether they were cued to a higher or lower rewarded stimulus), we wondered whether the modulation of theta-gamma P-A correlation with the attend-high versus attend-low condition was related to the firing rate modulation in the attend-high versus attend-low condition. We thus calculated the Attention Index for rate and P-A correlation in the same way as for the spatial attention condition, but for the different reward

conditions (where $\boldsymbol{AI_{rate}} = (firing_{high} - firing_{low}) / firing_{high} - firing_{low})$ as in **equation 9**, *and* $\mathbf{D_{reward}}$ is defined in **equation 8**)

Across all LFP pairs, we found only marginal positive correlations between D_{reward} and AI_{rate} for higher vs lower reward comparison, which were not significant (r=0.051, p = 0.135; after outlier removal: r=0.034, p = 0.325). Similarly, no correlation was significant when we computed them separately for phase providing LFPs from the individual subareas in PFC/ACC (VMPFC, lateral PFC, ACC, all p > 0.1) or for amplitude providing LFPs from the individual subareas in PFC/ACC (VMPFC, lateral PFC, ACC, all p > 0.5). Likewise, there were no significant correlations when restricting the correlation analysis to neurons with large or small attentional firing rate modulations.

In conclusion, we did not find a prominent association of target value specific firing rate modulation and target value specific cross-frequency P-A correlations.

4.2 - The relation of theta-gamma LFP-LFP correlations and burst-LFP synchronization

In a previous study we have shown that the local field potentials in ACC and lateral PFC synchronized long-range at narrow frequency bands of the LFP to burst firing events of single isolated neurons (Womelsdorf et al., 2014a). This previous analysis was based on the same dataset and anatomical reconstruction of recording sites as used here, but included a smaller subset of all LFP recording sites based on whether they were recorded simultaneously with single (spiking and bursting) neurons. Based on these previous insights, we were interested in whether the increase in theta-gamma LFP-LFP cross frequency correlation following the attention cue that we report here is related to the previously reported inter-areal burst-LFP synchronization.

In particular, the previous study reported that burst firing events in about one third of single neurons synchronized bursts to remote LFP activity at 15-25 Hz β band frequencies, and another third of neurons synchronized bursts to LFPs at a mid-range 50-75 Hz gamma frequency band (the last third of burst firing neurons did not show synchronization). In addition, we reported as a secondary finding in the previous manuscript that about a quarter of those neurons with burst synchronization at beta- and gamma- band frequency also showed significant synchronization of burst firing events to a 5-10 Hz theta frequency band of the LFP at remote sites (*see* Supplementary Figures S5 in (Womelsdorf et al., 2014a)).

Based on these previous findings, we tested whether there was any relationship between theta-gamma P-A correlation in the 500 ms post-cue period and the strength of burst synchronization in the same epoch. We (1) selected for this analysis the three frequency ranges for which burst-LFP synchronization was reliably shown (5-10 Hz theta, 15-25 Hz low-beta, and 50-75 Hz mid-gamma frequencies), (2) calculated the average burst-LFP synchronization for each frequency band, and (3) calculated Spearman rank correlations between the strength of burst-LFP synchronization and LFP-LFP theta-gamma phase amplitude correlations (for details see Methods). We summarize 3 major findings below and report the results of all correlations in **Table 1**.

Firstly, we found that in those LFP channels that provided the theta-phases for significantly theta-gamma P-A correlated channels, single neurons showed stronger burst-LFP synchronization to gamma frequency activity at remote channels (Spearman rank correlation, $r = 0.20$, $p = 0.044$, uncorrected for multiple comparisons, **Table 1**). This finding suggests that the existence of reliable (i.e. significant) theta-gamma cross-frequency interactions between two channels may also allow inference of burst firing events in the theta-phase providing LFP

channels likewise coupled to remote gamma events. In other words, task-modulated, inter-areal coupling of theta LFP activities to remote narrow LFP band gamma activity may translate to inter-areal coupling of burst events to remote narrow band LFP gamma activity.

Secondly, we found a second, significant positive correlation indicating that theta-phases in LFP channels donating gamma during theta-gamma correlations were synchronized to remote burst events (Spearman rank correlation, $r = 0.072$, $p = 0.027$, uncorrected for multiple comparisons, **Table 1**). This finding suggests that LFP channels with gamma activity that was modulated by remote LFP theta phases (*see* Results), also locked remote burst events via theta-phase modulation.

Thirdly, beyond the two positive correlations of theta-gamma P-A correlations and burst synchronization, we found two negative relationships that suggest a decoupling of theta-gamma interactions of LFPs and burst events from activity at beta frequencies (marked in blue font in **Table 1**). LFP channels that were participating in reliable (significant) theta-gamma cross-frequency interactions showed lower LFP β frequency synchronization with burst events from remote channels (theta phase providing LFPs: $r= -0.246$, $p = 0.016$, uncorrected for multiple comparisons; gamma amplitude providing LFPs: $r = -0.219$, $p = 0.032$, uncorrected for multiple comparisons). This finding suggests that LFPs with theta-gamma interactions are not engaged at the same time as beta frequency modulations.

These findings provide first quantitative evidence that recording sites with LFP theta-phases that engage in long-range gamma correlations also host neurons whose burst firing events synchronize long-range to gamma activity.

CHAPTER 5: DISCUSSION & CONCLUSION

5.1 - Discussion

The main result of the present work is that a centrally presented attention cue induces a correlation of 5-10 Hz theta band phase fluctuations and 35-55 Hz gamma band activations between cortical subfields in ACC/PFC. This theta-gamma phase-amplitude correlation was weaker on erroneous trials that correct trials and thus signified successful shifts of attention, i.e. cue utilization. On error trials, preferred theta phases were earlier and more variable in the theta cycle compared to correct trials. This suggests that failures of shifting attention are associated with the de-coherence of theta to gamma interactions in a network comprising the ACC/PFC. In this network, the theta-gamma P-A correlations were supported disproportionally often by theta phases from within the ACC as compared to the lateral PFC. This finding indicates that it is particularly the ACC (the rostral part of area 24) that provides a critical, slow theta-periodic influence on gamma mediated processes within the lateral PFC during the implementation of attention shifts. A further major characteristic of theta-gamma correlation is its close association with a cue-induced theta-phase reset. More than one-third of phase providing LFPs for significant theta-gamma P-A correlation showed the largest theta phase consistency within the first 0.3 sec. following cue onset, suggesting that a theta-phase reset could mechanistically be a source of anatomically widespread theta-gamma correlation. Taken together, these findings provide a novel perspective on how the control of attention is implemented by circuits in primate ACC/PFC and corroborate a long-held hypothesis that theta-gamma cross-frequency interactions are an essential means of inter-areal integration of distributed activities in multi-node cortical networks (Lisman and Jensen, 2013; Mcginn and Valiante, 2014).

5.1.1 - Frequency specificity of phase-amplitude correlation in ACC/PFC.

Our main finding characterized the statistical relation of two band-limited activity fluctuations comprising a narrow ~5-10 Hz (peak at 7 Hz) theta band and a ~35-55 Hz (peak at 40 Hz) gamma band. Previous studies have documented that a 5-10 Hz theta band is a widespread LFP signature in ACC/PFC that increases with specific demands to control goal-directed behaviour (Tsujimoto et al., 2010b; Womelsdorf et al., 2010; Liebe et al., 2012; Phillips et al., 2013). Our study corroborates these reports (**Fig. A5**), revealing correct attentional control is associated with distributed bursts of gamma activity in ACC/PFC that align to preferred phases of the theta oscillation. This further supports the notion that theta-gamma P-A correlation is a ubiquitous phenomenon evident across multiple circuits, including hippocampal-neocortical circuits (Colgin et al., 2009), hippocampal-striatal networks (Tort et al., 2008), cortico-striatal networks (von Nicolai et al., 2014) and cortico-cortical networks (Canolty et al., 2010; Bosman et al., 2012). Our results extend the role of theta-gamma P-A correlation to PFC circuits, with ~35% of LFP sites contributing to significant theta-gamma interactions. However, these sites show anatomically specific clustering, with a moderate maximal ~8-10% of inter-areal ACC-theta to LPFC-gamma pairs showing individually significant effects (**Fig. 5**).

In previous studies, 5-10 Hz activity fluctuations were shown to organize distinct band limited gamma frequency bands categorized as low (~35-55 Hz), medium (~50-90 Hz) and high (epsilon; ~90-140 Hz) bands, each likely originating in separable underlying circuit motifs (Colgin et al., 2009; Lisman and Jensen, 2013; Womelsdorf et al., 2014b). The observation that ACC/PFC circuits theta-synchronized the activation at a low-gamma frequency band (35-55 Hz) is to our knowledge unprecedented in LFP recordings in the primate brain. However, a similar theta to low-gamma P-A correlation has been found in rodents to emerge in medial frontal,

entorhinal, and hippocampal circuits (Tort et al., 2008; Colgin et al., 2009; Lisman and Jensen, 2013; Shearkhani and Takehara-Nishiuchi, 2013). In the cortex of nonhuman primates, synchronization of a low (35-55 Hz) gamma frequency band has recently been described to characterize local LFP and spike-LFP coherence *within* the macaque frontal eye field (FEF) during sustained selective attention (Gregoriou et al., 2009) (for a lower 30-40 Hz beta/gamma in lateral PFC, *see* (Siegel et al., 2009)). The cortical ACC/PFC fields engaging in theta-locked low-gamma activation in our study anatomically connect to the FEF. This makes it likely that the observed theta-phase reset in ACC/PFC also synchronizes FEF gamma activity bursts and spiking activity of visually selective FEF neurons that most strongly synchronize to the local, low gamma activity in FEF during sustained selective attentional processing (Gregoriou et al., 2012). Thus, the band-limited neuronal activation of the specific theta and gamma bands that interact during attention shifts in our study may serve as general band-limited signatures of neuronal coordination of attention information during goal-directed behaviors.

5.1.2 - Functional significance of theta-phase resets in the ACC/PFC.

The observed attention-cue triggered P-A correlations were associated with a prominent theta-phase reset. Similar to the absence of theta-gamma P-A correlation on error trials, the theta phase failed to reset following the attention cue on error trials (**Fig. 6B**), illustrating that the LFP theta-phase resets of the theta-gamma correlated network also indexed whether attention shifts are successful. A plausible mechanism for such a far reaching consequence of phase aligned theta activation can be found in recent studies that identified how a cue-induced phase reset effectively gates the outflow of a cortical circuit (Rizzuto et al., 2003; McCartney et al., 2004; Courtin et al., 2013). These studies suggest that the phase-reset-gated output of a local circuit can

serve as the causal trigger of distant gamma activity phase locked to theta activity. For example, one optogenetic study documented that a locally-generated theta-phase reset in rodent frontal cortices develops in conjunction with learning the meaning of a (classically conditioned) cue (Courtin et al., 2013). Following learning, the cue-triggered theta-phase reset predicted when projection neurons phase lock their spike output to the peak of theta oscillation cycles (Courtin et al., 2013). Moreover, the theta-phase reset effectively synchronized the spiking activity of those projection neurons in rodent medial PFC that activated fear related target structures that modified behavior. The reported attention-cue induced phase reset may be analogous to such a sequence of events. In our task, the cue signified a color matching rule ('*find the peripheral stimulus matching the color of the cue and enhance its representation against other stimuli*'). Correctly interpreting the cue required re-activating neural assemblies coding for the rule representation and applying the rule to the visually available information to eventually prioritize processing of the attended stimulus and filter out un-cued stimuli ((Kaping et al., 2011; Buschman et al., 2012); *see* **Fig. A8A**). Such an attentional remapping of functional connectivity occurred in the first 500 ms following attention cue onset (Kaping et al., 2011), and it is during this process that theta phases were most consistent across trials and began to synchronize remote gamma activities across ACC/PFC. It is therefore possible that the cue-triggered theta reset is instrumental to synchronize ACC/PFC neural circuits to theta rhythmic, ~140ms long activation periods that provide a reference for phase-locked gamma activity bursts.

Three additional sources of evidence support this prediction and are in line with our results. Firstly, studies in rodents suggest that theta-phase resets and theta coupling to gamma emerges in a prefrontal-hippocampal network to widely varying types of instructional cues, ranging from (Pavlovian-) cues in classical conditioning contexts (Courtin et al., 2013;

Shearkhani and Takehara-Nishiuchi, 2013), to instrumental cues in spatial choice tasks and item-context association tasks (Tort et al., 2008; Benchenane et al., 2010). Secondly, computational studies have identified canonical circuit motifs of theta-gamma correlation in which the theta phase can be instrumental in triggering and even generating gamma band activities in postsynaptic target circuits (Neymotin et al., 2013; Onslow et al., 2014). Key assumptions of such '*theta reset models'* are the existence of a robust gamma generating feedback circuit in the target structure, and a low frequency (theta periodic) modulated input to inhibitory cells in the circuit (Wulff et al., 2009; Pastoll et al., 2013; Onslow et al., 2014). This low frequency (theta) modulated input may likewise be generated de-novo from within the circuit from theta-generating or theta-resonating interneuron populations (*see* Fig. 1A in (Womelsdorf et al., 2014b); *see* **Fig. A8** for other Dynamic Circuit Motifs). Thirdly, a large set of studies have documented how attentional expectancies re-align phases of low frequencies in sensory cortices to the time when attentionally relevant stimuli are expected to occur in order to support goal directed behavior (Van Atteveldt et al., 2014). Such *anticipatory* phase entrainment resembles 'resets' and can synchronize high frequency activities at beta and gamma bands which correlate with sensory detection speed and the efficiency of subjects to filter out distractors in attention tasks (Bonnefond and Jensen, 2012; Van Atteveldt et al., 2014). Consistent with these findings, in a situation without externally imposed entrainment of rhythmic events, attention cues induce a rapid phase reset and thereby possibly implement a covert selection of relevant sensory stimuli according to the cue-dependent instructional rule.

5.1.3 - Theta-gamma correlation as a means to coordinate attention information.

It is important to acknowledge that the theta-phase reset and theta-gamma P-A correlation

was found in precisely those cortical circuits of the ACC/PFC which are functionally essential for the flexible control and biasing of attention and goal directed behavior (Passingham and Wise, 2012; Miller and Buschman, 2013). To realize such a control/bias function, ACC/PFC likely continuously interact with fronto-parietal attention networks during goal-directed behavior to ensure continued attention to relevant information that relate to the task goals and other working memory contents (Miller and Buschman, 2013; Shenhav et al., 2013). Such biasing during attentive processes is realized through theta-gamma cross-frequency interactions involving circuits in ACC/PFC.

An important piece of information supporting the proposed '*P-A correlation hypothesis of attentional control*' is the relationship between burst spiking events and theta-gamma correlation. Burst firing of neurons synchronized to remote gamma band activity at those LFP recording channels that provided the theta-phases for LFP pairs with significant theta-gamma correlation. This result links findings on inter-areal burst synchronization (Womelsdorf et al., 2014a) with the current report of functionally relevant theta-gamma correlations and suggests that inter-areal theta-gamma interactions of different LFPs may directly or indirectly relate to burst firing of neurons within the theta-frequency modulated circuits. Intriguingly, firing of bursts or firing of sequences during brief periods of theta-nested gamma band activity is strongly implicated in rodent hippocampus and striatum to carry unique information about internally maintained goals (e.g. the location of the most rewarded outcome) (Gupta et al., 2012; Pezzulo et al., 2014). Our results suggest that theta nested gamma modulations may serve as a means to organize and integrate such covertly (internally) generated information to ensure the flexible control of attention during goal-directed behaviors.

5.2 - Conclusion

Oscillatory activity has long been recognized as a key signature of cognition and brain operation. However, it is increasingly acknowledged that band-limited rhythmicity in the brain not only modulates cortical operations, but may also be the mechanistic basis for information coordination across sensory, motor, and cognitive systems (Fries, 2005; Buzsaki, 2006; Buzsáki, 2010; Lisman and Jensen, 2013; Van Atteveldt et al., 2014). In my Master's work, I have evaluated meso-scale signals of oscillatory coordination in light of behavioral function, and demonstrated their relation to single cell activity. Co-activation of theta phase and gamma amplitude emerged specifically in those areas of the frontal cortex responsible for shifting attention, with theta phase emerging in ACC and gamma amplitude emerging in LPFC. This P-A correlation is likely driven by a theta-phase reset that emerges in relation to an external cue and aligns theta-oscillations in order to route information necessary for correct attention shifts. I have also shown that bursts in nodes where theta-phase is prevalent also couple to distant mid-gamma in relation to the strength of theta-(low) gamma correlation.

Although I have performed many control analyses to demonstrate that P-A correlation is indeed relevant to performance, there are still some considerations that must be evaluated. Cross-frequency correlation has been extensively studied in rodents, where oscillations are robust over many cycles (Buzsaki, 2006). However, rhythmic activity in primates generally lasts for only a few cycles, and our study is no exception; during cross frequency coordination, we observed theta persisting for ~2 cycles. Multiple pieces of evidence point to the existence of a true theta-rhythmic component in the signal. First, I observed a peak in the spectrogram at theta, suggesting the existence of theta-rhythmic activity. Second, it may be possible that theta-gamma correlation persists because of an event related transient that leads to artifactual activity in the theta band. In such a case, theta-gamma coordination (on correct but not error trials) would be an artifact, and

we would expect event related transients to be different on correct and error trials as well. However, event related transients (determined using statistically sensitive cluster based permutation test) were similar on correct and error trials, whereas both theta phase consistency and theta-gamma correlation accounted for behavior. This also suggests that a theta-rhythmic component in the signal exists and is behaviorally relevant.

It is possible that theta activity was instantiated by the onset of the color cue before attention cue came online. These pre-cue effects may have an indirect influence on the cue induced theta - gamma correlation, that we did not explicitly control for. However, it is unlikely that pre-cue effects had a systematic effect on the attention cue triggered response because the color onset was jittered within 50-700 ms prior to the attention cue onset. Future analysis should take into account possible influences from average field effects to quantify possible contributions of attention cues and other types of cues such as the reward outcome 'cue' that the color of the stimuli in our experiments conveyed.

The MI requires relatively long recordings (consisting of more than a few thousand time samples) to avoid spurious results. Our task design required concatenation of trials in order to achieve such long data samples. This precludes us from inferring function of P-A correlation on a trial-by-trial basis. Yet coordination of information occurs at such a scale, and there are some studies suggesting that P-A correlation is an index of learning across trials (Tort et al., 2009). Testing this in our experiments would require the development of P-A correlation metrics that are more sensitive to short time sample.

Another important consideration is the nature of the observed phase-reset . Our results are in accordance with literature suggesting that a phase reset can be inferred when evaluating both the power and phase consistency of (theta band) oscillations. I have demonstrated that 5-10 Hz

power is evident as a peak in the spectral plot before attention cue onset, and remains constant after attention cue onset. On the other hand, LFPs providing theta phase also showed phase consistency across correct trials, but not error trials. Moreover, time-locked event related transients were statistically similar on both correct and error trials, suggesting event transients could not account for behavior, whereas phase consistency does. This suggests that the phenomenon was a "true" phase reset, as opposed to a phenomenon driven by non-stationary effects. However, it is still possible that within each LFP, the phase reset is driven by new oscillators that are recruited after attention cue onset (Sauseng et al., 2007; Ding and Simon, 2013). Conclusively showing that this is not the case would require analysis of dense single cell recordings, showing that activity in each does not represent recruitment of new oscillators. This could also be addressed via causal manipulations (e.g. optogenetics) that induce or inhibit oscillations, with a measureable effect on behavior. This has been achieved in a recent study in rodents, suggesting that phase resets occur in relation to internal signals that re-organize theta oscillations (Courtin et al., 2013).

I have also shown that bursts coupled to distal gamma co-occur in LFPs that phase reset. Bursts can serve as a strong activator of post-synaptic depolarization, which could lead to theta-phase realignment (i.e. theta phase reset). On the other hand, theta oscillations represent periods of high and low excitability, suggesting that bursts may occur during the duty cycle of theta oscillations when pre-synaptic impulses are most effective in initiating bursts. Importantly, this implies that both the phase reset and bursts may be the mechanistic source of network formation, as shown in this work and also by Womelsdorf and colleagues (Womelsdorf et al., 2014a). Put another way, external cues that drive network coordination may do so via either a phase reset or burst activity. Dissociating these possibilities is an important future direction of study.

Finally, although I report that theta-gamma coordination supports attention shifts, this still leaves open the question of how specific information about the target (e.g. spatial location, reward value, color) is represented in the framework of theta-gamma interactions. I have shown that it is possible for theta-gamma correlation to dissociate, at least in some nodes, differences in value or spatial location. These nodes are largely distinct from those predictive of correct attention shifts, though theta-gamma correlation increases after attention cue onset for both different reward values, and different spatial locations. Thus, theta-gamma interactions may facilitate coordination of information in different circuits that subserve different decision related functions. Importantly, target characteristics may be encoded in yet other frequency bands that may be complementary conduits for feed-forward and feedback information across the cortex(Buschman et al., 2012; Bastos et al., 2014). A critical avenue for future research is thus localizing neural ensembles that encode target features, and determining what (if any) cross-frequency interactions support them.

This study represents the first comprehensive characterization of P-A coupling in primate ACC/PFC that supports attention. P-A correlation is predictive of attentional deployment in support of correct behavior. Aberrant oscillations are prevalent in pathological conditions such as attention deficit disorder and schizophrenia (Bush, 2009; Carter et al., 2010), suggesting that symptoms may emerge because of improper coordination. Thus, a critical next step is determining if the findings of this work may be replicated in humans, which would imply that P-A correlation may be a tool for detecting and possibly manipulating functional networks supporting cognition.

BIBLIOGRAPHY

Ardid S, Vinck M, Kaping D, Marquez S, Everling S, Womelsdorf T (2015) Mapping of functionally characterized cell classes onto canonical circuit operations in primate prefrontal cortex. J Neurosci 35:2975–2991.

Aru J, Priesemann V, Wibral M, Lana L, Pipa G, Singer W, Vicente R (2015) Untangling cross-frequency coupling in neuroscience. Curr Biol 31:51–61.

Averbeck BB, Seo M (2008) The statistical neuroanatomy of frontal networks in the macaque. PLoS Comput Biol 4:1–11.

Barbas H (2015) General Cortical and Special Prefrontal Connections: Principles from Structure to Function. Annu Rev Neurosci 38:269–289.

Barbas H, Zikopoulos B (2007) The prefrontal cortex and flexible behavior. Neuroscientist 13:532–545.

Bastos AM, Vezoli J, Bosman CA, Schoffelen J-M, Oostenveld R, Dowdall JR, De Weerd P, Kennedy H, Fries P (2014) Visual Areas Exert Feedforward and Feedback Influences through Distinct Frequency Channels. Neuron 85:390–401.

Behrens TEJ, Woolrich MW, Walton ME, Rushworth MFS (2007) Learning the value of information in an uncertain world. Nat Neurosci 10:1214–1221.

Benchenane K, Peyrache A, Khamassi M, Tierney PL, Gioanni Y, Battaglia FP, Wiener SI (2010) Coherent Theta Oscillations and Reorganization of Spike Timing in the Hippocampal- Prefrontal Network upon Learning. Neuron 66:921–936.

Berens P (2009) CircStat: A MATLAB toolbox for circular statistics. J Stat Softw 31:1–21.

Bieri KW, Bobbitt KN, Colgin LL (2014) Slow and Fast Gamma Rhythms Coordinate Different Spatial Coding Modes in Hippocampal Place Cells. Neuron 82:670–681.

Bonnefond M, Jensen O (2012) Alpha oscillations serve to protect working memory maintenance against anticipated distracters. Curr Biol 22:1969–1974.

Bosman C a, Schoffelen J-M, Brunet N, Oostenveld R, Bastos AM, Womelsdorf T, Rubehn B, Stieglitz T, De Weerd P, Fries P (2012) Attentional stimulus selection through selective synchronization between monkey visual areas. Neuron 75:875–888.

Buschman TJ, Denovellis EL, Diogo C, Bullock D, Miller EK (2012) Synchronous oscillatory neural ensembles for rules in the prefrontal cortex. Neuron 76:838–846.

Bush G (2009) Attention-Deficit/Hyperactivity Disorder and Attention Networks. Neuropsychopharmacology 35:278–300.

Buzsaki G (2006) Rhythms of the Brain. Oxford University Press.

Buzsáki G (2010) Neural syntax: cell assemblies, synapsembles, and readers. Neuron 68:362–385.

Buzsáki G, Logothetis N, Singer W (2013) Scaling brain size, keeping timing: Evolutionary preservation of brain rhythms. Neuron 80:751–764.

Canolty RT, Ganguly K, Kennerley SW, Cadieu CF, Koepsell K, Wallis JD, Carmena JM (2010) Oscillatory phase coupling coordinates anatomically dispersed functional cell assemblies. Proc Natl Acad Sci U S A 107:17356–17361.

Canolty RT, Knight RT (2010) The functional role of cross-frequency coupling. Trends Cogn Sci 14:506–515.

Carter JD, Bizzell J, Kim C, Bellion C, Carpenter KLH, Dichter G, Belger A (2010) Attention deficits in schizophrenia--preliminary evidence of dissociable transient and sustained deficits. Schizophr Res 122:104–112.

Cavanagh JF, Cohen MX, Allen JJB (2009) Prelude to and resolution of an error: EEG phase synchrony reveals cognitive control dynamics during action monitoring. J Neurosci 29:98–105.

Cavanagh JF, Frank MJ (2014) Frontal theta as a mechanism for cognitive control. Trends Cogn Sci 18:414–421.

Cavanagh JF, Frank MJ, Klein TJ, Allen JJB (2010) Frontal theta links prediction errors to behavioral adaptation in reinforcement learning. Neuroimage 49:3198–3209.

Colgin LL, Denninger T, Fyhn M, Hafting T, Bonnevie T, Jensen O, Moser M-B, Moser EI (2009) Frequency of gamma oscillations routes flow of information in the hippocampus. Nature 462:353–357.

Courtin J, Chaudun F, Rozeske RR, Karalis N, Gonzalez-Campo C, Wurtz H, Abdi A, Baufreton J, Bienvenu TCM, Herry C (2013) Prefrontal parvalbumin interneurons shape neuronal activity to drive fear expression. Nature 505:92–96.

Ding N, Simon JZ (2013) Power and phase properties of oscillatory neural responses in the presence of background activity. J Comput Neurosci 34:337–343.

Engel AK, Fries P (2010) Beta-band oscillations-signalling the status quo? Curr Opin Neurobiol 20:156–165.

Fries P (2005) A mechanism for cognitive dynamics: neuronal communication through neuronal coherence. Trends Cogn Sci 9:474–480.

Genovesio A, Wise SP, Passingham RE (2014) Prefrontal-parietal function: From foraging to foresight. Trends Cogn Sci 18:72–81.

Glascher J, Adolphs R, Damasio H, Bechara a., Rudrauf D, Calamia M, Paul LK, Tranel D (2012) Lesion mapping of cognitive control and value-based decision making in the prefrontal cortex. Proc Natl Acad Sci 109:14681–14686.

Gregoriou GG, Gotts SJ, Desimone R (2012) Cell-type-specific synchronization of neural activity in FEF with V4 during attention. Neuron 73:581–594.

Gregoriou GG, Gotts SJ, Zhou H, Desimone R (2009) High-frequency, long-range coupling between prefrontal and visual cortex during attention. Science 324:1207–1210.

Gupta AS, van der Meer M a a, Touretzky DS, Redish a D (2012) Segmentation of spatial experience by hippocampal theta sequences. Nat Neurosci 15:1032–1039.

Hayden BY, Heilbronner SR, Pearson JM, Platt ML (2011) Surprise signals in anterior cingulate cortex: neuronal encoding of unsigned reward prediction errors driving adjustment in behavior. J Neurosci 31:4178–4187.

Huxter JR, Senior TJ, Allen K, Csicsvari J (2008) Theta phase-specific codes for two-dimensional position, trajectory and heading in the hippocampus. Nat Neurosci 11:587–594.

Jensen O, Colgin LL (2007) Cross-frequency coupling between neuronal oscillations. Trends Cogn Sci 11:267–269.

Kaping D, Vinck M, Hutchison RM, Everling S, Womelsdorf T (2011) Specific contributions of ventromedial, anterior cingulate, and lateral prefrontal cortex for attentional selection and stimulus valuation. PLoS Biol 9.

Kennerley SW, Walton ME, Behrens TEJ, Buckley MJ, Rushworth MFS (2006) Optimal decision making and the anterior cingulate cortex. Nat Neurosci 9:940–947.

Liebe S, Hoerzer GM, Logothetis NK, Rainer G (2012) Theta coupling between V4 and prefrontal cortex predicts visual short-term memory performance. Nat Neurosci 15:456–462, S1–S2.

Lisman J, Jensen O (2013) The theta-gamma neural code. Neuron 77:1002–1016.

Maris E, Oostenveld R (2007) Nonparametric statistical testing of EEG- and MEG-data. J Neurosci Methods 164:177–190.

Matsumoto M, Matsumoto K, Abe H, Tanaka K (2007) Medial prefrontal cell activity signaling prediction errors of action values. Nat Neurosci 10:647–656.

McCartney H, Johnson AD, Weil ZM, Givens B (2004) Theta reset produces optimal conditions for long-term potentiation. Hippocampus 14:684–687.

Mcginn RJ, Valiante XT a (2014) Phase – Amplitude Coupling and Interlaminar Synchrony Are Correlated in Human Neocortex. 34:15923–15930.

Miller EK, Buschman TJ (2013) Cortical circuits for the control of attention. Curr Opin Neurobiol 23:216–222.

Neymotin S a., Hilscher MM, Moulin TC, Skolnick Y, Lazarewicz MT, Lytton WW (2013) Ih Tunes Theta/Gamma Oscillations and Cross-Frequency Coupling In an In Silico CA3 Model. PLoS One 8.

O'Keefe J, Recce ML (1993) Phase relationship between hippocampal place units and the EEG theta rhythm. Hippocampus 3:317–330.

Onslow ACE, Jones MW, Bogacz R (2014) A canonical circuit for generating phase-amplitude coupling. PLoS One 9:e102591.

Oostenveld R, Fries P, Maris E, Schoffelen JM (2011) FieldTrip: Open source software for advanced analysis of MEG, EEG, and invasive electrophysiological data. Comput Intell Neurosci 2011.

Passingham RE, Wise SP (2012) The Neurobiology of the Prefrontal Cortex: Anatomy, Evolution, and the Origin of Insight. Oxford University Press.

Pastoll H, Solanka L, van Rossum MCW, Nolan MF (2013) Feedback inhibition enables θ-nested γ oscillations and grid firing fields. Neuron 77:141–154.

Petrides M, Pandya DN (2007) Efferent association pathways from the rostral prefrontal cortex in the macaque monkey. J Neurosci 27:11573–11586.

Pezzulo G, van der Meer M a a, Lansink CS, Pennartz CM a (2014) Internally generated sequences in learning and executing goal-directed behavior. Trends Cogn Sci:1–11.

Phillips JM, Vinck M, Everling S, Womelsdorf T (2013) A Long-Range Fronto-Parietal 5- to 10-Hz Network Predicts "Top-Down" Controlled Guidance in a Task-Switch Paradigm. Cereb cortex.

Rizzuto DS, Madsen JR, Bromfield EB, Schulze-Bonhage A, Seelig D, Aschenbrenner-Scheibe R, Kahana MJ (2003) Reset of human neocortical oscillations during a working memory task. Proc Natl Acad Sci U S A 100:7931–7936.

Rossi AF, Bichot NP, Desimone R, Ungerleider LG (2007) Top down attentional deficits in macaques with lesions of lateral prefrontal cortex. J Neurosci 27:11306–11314.

Rothé M, Quilodran R, Sallet J, Procyk E (2011) Coordination of high gamma activity in anterior cingulate and lateral prefrontal cortical areas during adaptation. J Neurosci 31:11110–11117.

Rudebeck PH, Behrens TE, Kennerley SW, Baxter MG, Buckley MJ, Walton ME, Rushworth MFS (2008) Frontal cortex subregions play distinct roles in choices between actions and stimuli. J Neurosci 28:13775–13785.

Rushworth MFS, Noonan MP, Boorman ED, Walton ME, Behrens TE (2011) Frontal cortex and reward-guided learning and decision-making. Neuron 70:1054–1069.

Salazar RF, Dotson NM, Bressler SL, Gray CM (2012) Content-Specific Fronto-Parietal Synchronization During Visual Working Memory. Science (80-) 338:1097–1100.

Saleem KS, Kondo H, Price JL (2008) Complementary circuits connecting the orbital and medial prefrontal networks with the temporal, insular, and opercular cortex in the macaque monkey. J Comp Neurol 506:659–693.

Sauseng P, Klimesch W, Gruber WR, Hanslmayr S, Freunberger R, Doppelmayr M (2007) Are event-related potential components generated by phase resetting of brain oscillations? A critical discussion. Neuroscience 146:1435–1444.

Schroeder CE, Lakatos P (2009) Low-frequency neuronal oscillations as instruments of sensory selection. Trends Neurosci 32:9–18.

Shearkhani O, Takehara-Nishiuchi K (2013) Coupling of prefrontal gamma amplitude and theta phase is strengthened in trace eyeblink conditioning. Neurobiol Learn Mem 100:117–126.

Shen C, Ardid S, Kaping D, Westendorff S, Everling S, Womelsdorf T (2014) Anterior Cingulate Cortex Cells Identify Process-Specific Errors of Attentional Control Prior to Transient Prefrontal-Cingulate Inhibition. Cereb Cortex.

Shenhav A, Botvinick MM, Cohen JD (2013) The Expected Value of Control: An Integrative Theory of Anterior Cingulate Cortex Function. Neuron 79:217–240.

Siegel M, Warden MR, Miller EK (2009) Phase-dependent neuronal coding of objects in short-term memory. Proc Natl Acad Sci 106:21341–21346.

Sirota A, Montgomery S, Fujisawa S, Isomura Y, Zugaro M, Buzsáki G (2008) Entrainment of Neocortical Neurons and Gamma Oscillations by the Hippocampal Theta Rhythm. Neuron 60:683–697.

Tort ABL, Komorowski R, Eichenbaum H, Kopell N (2010) Measuring phase-amplitude coupling between neuronal oscillations of different frequencies. J Neurophysiol 104:1195–1210.

Tort ABL, Komorowski RW, Manns JR, Kopell NJ, Eichenbaum H (2009) Theta-gamma coupling increases during the learning of item-context associations. Proc Natl Acad Sci U S A 106:20942–20947.

Tort ABL, Kramer MA, Thorn C, Gibson DJ, Kubota Y, Graybiel AM, Kopell NJ (2008) Dynamic cross-frequency couplings of local field potential oscillations in rat striatum and hippocampus during performance of a T-maze task. Proc Natl Acad Sci U S A 105:20517–20522.

Tremblay S, Pieper F, Sachs A, Martinez-Trujillo J (2015) Attentional Filtering of Visual Information by Neuronal Ensembles in the Primate Lateral Prefrontal Cortex. Neuron 85:202–215.

Tsujimoto S, Genovesio A, Wise SP (2010a) Evaluating self-generated decisions in frontal pole cortex of monkeys. Nat Neurosci 13:120–126.

Tsujimoto T, Shimazu H, Isomura Y (2006) Direct recording of theta oscillations in primate prefrontal and anterior cingulate cortices. J Neurophysiol 95:2987–3000.

Tsujimoto T, Shimazu H, Isomura Y, Sasaki K (2010b) Theta oscillations in primate prefrontal and anterior cingulate cortices in forewarned reaction time tasks. J Neurophysiol 103:827–843.

Van Atteveldt N, Murray MM, Thut G, Schroeder CE (2014) Multisensory integration: Flexible use of general operations. Neuron 81:1240–1253.

Van der Meij R, Kahana M, Maris E (2012) Phase-amplitude coupling in human electrocorticography is spatially distributed and phase diverse. J Neurosci 32:111–123.

Varela F, Lachaux J, Rodriguez E, Martinerie J (2001) The Brainweb: Phase Synchronization and Large-Scale Integration. Nat Rev Neurosci 2:229–239.

Von Nicolai C, Engler G, Sharott A, Engel AK, Moll CK, Siegel M (2014) Corticostriatal Coordination through Coherent Phase-Amplitude Coupling. J Neurosci 34:5938–5948.

Von Stein a, Sarnthein J (2000) Different frequencies for different scales of cortical integration: from local gamma to long range alpha/theta synchronization. Int J Psychophysiol 38:301–313.

Womelsdorf T, Ardid S, Everling S, Valiante TA (2014a) Burst Firing Synchronizes Prefrontal and Anterior Cingulate Cortex during Attentional Control. Curr Biol:1–9.

Womelsdorf T, Fries P (2007) The role of neuronal synchronization in selective attention. Curr Opin Neurobiol 17:154–160.

Womelsdorf T, Johnston K, Vinck M, Everling S (2010) Theta-activity in anterior cingulate cortex predicts task rules and their adjustments following errors. Proc Natl Acad Sci U S A 107:5248–5253.

Womelsdorf T, Valiante T a, Sahin NT, Miller KJ, Tiesinga P (2014b) Dynamic circuit motifs underlying rhythmic gain control, gating and integration. Nat Neurosci 17:1031–1039.

Wulff P, Ponomarenko A a, Bartos M, Korotkova TM, Fuchs EC, Bähner F, Both M, Tort ABL, Kopell NJ, Wisden W, Monyer H (2009) Hippocampal theta rhythm and its coupling with gamma oscillations require fast inhibition onto parvalbumin-positive interneurons. Proc Natl Acad Sci U S A 106:3561–3566.

Yeung N, Botvinick MM, Cohen JD (2004) The Neural Basis of Error Detection: Conflict Monitoring and the Error-Related Negativity. Psychol Rev 111:931–959.

Zar JH (2010) Biostatistical Analysis. Prentice Hall.

APPENDICES

APPENDIX A: SUPPLEMENTARY RESULTS

Result A1 - Results of LFP-LFP pairs from individual monkeys

For all primary results reported in the main text the LFP-LFP pairs were pooled from the individual monkeys. To ensure that the pooled results are qualitatively evident also in LFP-LFP pairs recorded from individual monkeys, I performed all analyses steps separately for each monkeys' LFP-LFP pairs and report the results below in the same succession as they are mentioned in the main text.

In summary, all primary results were qualitatively replicated for each monkey (points 1.1-1.4), and the majority of secondary (or control) results (points 1.5-1.9) likewise were replicated in individual monkeys.

Primary Results

1.1 – Theta-Gamma Correlation on Correct and Error trials

- Our main results show that (7 Hz) theta phase to (~40 Hz) gamma amplitude correlations between distant LFP pairs significantly increased after the attention cue onset on correct trials (**Fig 2A**). This theta-gamma correlation to significantly increase in **85** LFP pairs (7.7% of all LFP pairs) that were coming from both animals proportional to their overall number of LFP pairs. In monkey M **31/446** LFP pairs (**7.0%**) and in monkey R **54/658** LFP pairs (**8.2**%) showed significant theta-gamma correlation from pre- to post- attention cue. The overall significant increase in theta-gamma correlation across the restricted population of LFP pairs for individual monkeys was statistically significant for pairs of

monkey R (p=0.0045, FDR corrected), but did not reach significance across the smaller sample of n=31 LFP pairs of monkey M (p=1, FDR corrected).

- Compared to the increased theta-gamma correlations, a smaller total number of LFP pairs (n=46, 4.2%) showed individually significant decreases in the theta-gamma correlations from the pre- to post- attention cue periods. This decrease was evident in 15 LFP pairs (of 446 pairs, 3.4%) in monkey M and in 31 LFP pairs (of 658 pairs, 4.7%) in monkey R.
- On average there was no (7 Hz) theta to (~40Hz) gamma correlation on error trials (**Fig 2C**). In line with this average finding, there was no consistent increase in theta-gamma correlation on error trials in either monkey R (p = 1, FDR corrected), nor in monkey M (p= 0.63, FDR corrected).

1.2 - Theta Phase Preferences for Gamma Amplitude Modulation

- Pooled data showed that gamma correlations were evident in correct trials on average at theta phases around **-14.69^0**, 95% CI [-41.01^0, 11.63^0] (**Fig 3A**). The average phase on correct trials was similar in both animals: Monkey R's average phase on correct trials was **-24.93^0**, 95% CI [-48.60^0 -1.26^0]. Monkey M's average phase on correct trials was **-32.33^0**, 95% CI [-57.67^0 -122.33^0]. The phase distributions were significantly different from non-uniformity for the pooled data and for monkey R phases (p = 0.00017), but not for monkey M's phase distribution (p = 0.45).
- Compared to correct trials, the theta phases of the gamma amplitude modulations on error trials were more variable and shifted to more negative phases with an average theta phase for the pooled data of -94.28^0, 95% CI [-131.40^0, -57.16^0] (Fig 3B). A similar shift in mean phase was evident in monkey R (-97.61^0, 95% CI [-144.06^0 -51.17^0]) and in monkey M (-87.27, 95% CI [-177.27^0, 2.73^0]). Similar to the pooled distribution, none of

the phase distributions on error trials from individual monkeys were significantly different from a random distribution (Hodjes-Ajne test, all $p > 0.05$).

1.3 - Anatomical Distribution of Theta-Gamma Correlation

- For the pooled n=85 significant LFP pairs, LFP theta phase providing channels showed a preference for the ACC, and LFP gamma amplitude providing channels showed a preference for the LPFC, respectively (**Fig. 5D**). I separately quantified the anatomical origins of phase- and amplitude- providing channels for n=51 and n=31 LFP pairs with significant theta-gamma correlations for monkey R and monkey M respectively as the proportion of significant pairs relative to all recorded LFP pairs. I found the same trend in each of the monkeys. Both monkeys showed more theta phase providing channels in ACC than in lateral PFC (Monkey R: **9%** in ACC versus **3.5%** in lat. PFC; Monkey M: **9.7%** in ACC versus **3.2%** in lat. PFC). Similarly, both monkeys showed more gamma amplitude providing LFPs in lateral PFC than in the ACC (Monkey R: **5.9%** in lat. PFC versus **3.0%** in ACC; Monkey M: **10.5%** in lat PFC versus **3.2%** in lat. ACC). For VMPFC, the proportion of significant LFP pairs ranged from **4.6-10.7%** between monkeys and phase/amplitude LFP channel comparisons.

1.4 - Analysis of Theta Phase Reset

- A significant proportion of LFPs that showed theta-gamma P-A correlation increases during the attention shift period the theta-phases became more phase consistent across trials in the post-cue period on correct trials, but not on error trials (**Fig. 6D**). A similar result pattern was found in each monkey separately. In monkey R, **70% (35 of 50)** of the LFPs that donated theta to significant theta-gamma P-A correlation showed peak theta phase consistency in the (500 ms) post-cue period compared to the (500 ms) pre-cue

period on correct trials while there were less peaks in the post-cue period (**30%, 15 of 50**) on error trials. In monkey M, **75% (16 of 24)** of the LFPs showed peak theta phase consistency in the post-cue period on correct trials, while only **25% (8 of 24**) showed maximum phase consistency in the post cue period on error trials. The difference in proportions between pre-cue and post-cue period was significant in both monkeys on correct trials ($p<0.015$) but not error trials ($p>0.2$).

-

Secondary Results and Results from Control Analysis:

1.5 - Analysis of LFP Power

- In our pooled analysis, peaks in the LFP power spectra were evident in the theta frequency band in 73% of LFPs that engaged in P-A correlations, and that power modulations did not correlate with theta-gamma P-A correlation changes (**Result A3).** Both of these pooled findings were evident at the single monkey level. Monkey M and R showed a median theta-power peak (within ~5.5-8.5 Hz) of those LFPs that engaged in P-A correlations. In neither monkey did theta band power change from pre-post cue and thus did not correlate with the functional theta-gamma correlation increase (Spearman rank correlation, in either phase-or amplitude-providing LFPs, $p>0.20$).

1.6 - Average Cue-aligned Field Effects

- Similar to the pooled LFP average field effect, the LFP average field in each monkey showed no significant difference between the pattern of activation on correct trials, or on error trials (Monte Carlo surrogate test, all $p > 0.05$). Average peri-cue field potentials therefore cannot account for the functional pre- to post-cue changes .

1.7 - Theta Frequency Phase Coherence Analysis

- In the pooled data, the theta band phase coherence between areas in PFC did not change from pre-to post-cue and was not different in correct versus error trials (**Result A10**). The same results were found in each monkey. Both monkey's had a spectral peak of coherence at ~7 Hz ($p<0.05$ in monkey R, but $p>0.05$ in monkey M, FDR corrected), but this coherence did not change significantly from before to after attention cue onset.

1.8 - Temporal Jitter of Gamma Amplitude Phase to Theta versus Cue Onset Time

- Similar to the pooled results (**Result A4**), in both monkeys, the gamma peaks aligned more consistently to the phase of theta, rather than to the attention-cue onset (Monkey R: 47/54 LFP pairs, 87%; monkey M: 30/31 LFP pairs, 97%).

1.9 - Comparison of Trial Number Matched Correct and Error Trials

- In pooling data across monkeys, I found that correct trial MI changes were reliably higher than error trial MI changes (Monte Carlo surrogate test, evident in 968/1000 surrogates), when reducing the number of correct trials to that of error trials. Similar results were evident in each monkey independently. In both, the distribution of MI changes on correct trials was higher on average than the distribution of error MI changes (R: 54 LFP pairs = 767/1000 surrogates showed this trend; M: 31 LFP pairs = 770/1000 surrogates showed this trend).

Result A2 - Behavioral Analysis

Both animals performed the task at accuracy levels well above chance (R= 78.9 ± 0.9% SE, M= 86.7 ± 0.6% SE) across all (80/73 in monkey R/M) behavioural sessions of the monkeys.

This definition of accuracy takes into account all correctly performed trials. On the other hand, errors were defined as all other trials in which the animal maintained fixation on the central fixation point at least until the time of the cue onset. Thus, errors were committed during or after the selective attention period of the task.

Considering all these trials, both monkeys committed only 3.9/5.1% of errors during the 550 ms following a rotation of distractors (i.e. false positive errors) (R= 3.9 ± 0.2% SE, M= 5.1 ± 0.3% SE). Erroneous fixation breaks during the 550 ms after rotation of the cued target stimulus occurred in monkey R at 4.1 ± 0.2% SE, and for monkey M at 1.3 ± 0.1% SE). Incorrect saccadic responses to the rotation of the target stimulus occurred 3.4 ± 0.2% SE of the time for monkey R and 0.8 ± 0.1% SE for monkey M. Responses that were late or did not occur after 550 ms after the rotation onset occurred for monkey R at 8.3 ± 0.6% SE and for monkey M at 1.3 ± 0.2% SE. The remainder of error trials were fixation breaks between cue onset and onset of the first rotation (either of the distractor or the target stimulus).

Across experimental sessions, overall accuracy levels were higher for ipsilateral (left) than contralateral (right) cued target trials in monkey R (t-test, ipsilateral: 83.6 ± 0.7% SE; contralateral: R= 75.2 ± 1.2% SE, $p < 0.001$, t-test). Monkey M showed similar accuracy for ipsi- than contralaterally cued target trials and thus did not exhibit a bias (t-test, ipsi-lateral: M= 86.5 ± 0.6% SE, contra-lateral: M= 87.2 ± 0.8% SE, p= 0.511, respectively).

For the majority of sessions (70 of 80 sessions of monkey R, and 70 of 73 sessions of monkey M) attentional targets were differentially rewarded with 0.76 ml versus 0.4 ml. In these sessions, monkeys performed at high, above chance for both conditions, i.e. when cued to the higher rewarded target (R= 79.3%, SE=1.1, M= 89.0%, SE=0.7), and when cued to the lower rewarded target (R= 79.5 ± 1.0% SE, M= 85.4 ± 0.7% SE) with false alarm rates (responses

during the distractor rotations) between 3.3 and 5.7 % of all trials (for higher rewarded target trials: R= 3.3 ± 0.2% SE, M= 3.7 ± 0.3% SE; for lower rewarded target trials: R= 3.4 ± 0.2% SE, M= 5.7 ± 0.4% SE). For monkey R, the overall performance for high and low rewarded trials were statistically not different (t-test, p=0.858), while for monkey M accuracy was higher across sessions in trials that cued attention to high versus lower rewarded target stimuli (t-test, p=0.0004).

Result A3 - Analysis of LFP pairs showing significantly reduced theta-gamma correlation following attention cue onset

The main population effect was an increase in theta-gamma correlation in the post-cue compared to the pre-cue epoch (**Figure 3A,B**). In the main text, I characterized how the n=85 (7.7 %) LFP pairs with an individually significant theta-gamma increase in the post cue period evolve over time and in anatomical space. Despite the overall positive effect at the population level, a subset of n = 46 LFP pairs (4.2% of total pairs) that showed a significant reduction of theta-gamma correlation in the post-cue compared to the pre-cue period when tested at the individual LFP pair level. I therefore asked whether these LFP pairs were also modulated on error trials and whether they showed an anatomically distribution in ACC/PFC that was comparable to the LFP pairs with significant enhanced theta-gamma correlation.

Firstly, none of the LFP pairs with significantly reduced theta-gamma correlation on correct trials showed a significant reduction from pre-cue to post-cue on error trials. This finding could be due to lower cross-frequency correlation in the pre-cue period on error compared to correct trials, or it can be due to continuously enhanced cross-frequency correlation in the post-cue period on error trials, or a combination of both. I found that on error trials these LFP pairs

did not show significant theta-gamma correlation ($p > 0.05$) in the pre-cue period, revealing that the lack of reduction was dominated by already lower correlation prior to the cue.

Secondly, I next analyzed the anatomical distribution of LFP pairs showing significantly reduced theta-gamma correlations (similar to **Fig. 5**). There was no anatomical specificity of the distribution of LFP phase providing channels and LFP amplitude providing channels for these n=46 LFP pairs with only one exception: There was a significant smaller than expected number of phase-amplitude LFP pairs with reduced theta-gamma correlations from VMPFC to ACC than would be expect by chance. These anatomical results suggest that LFP pairs with theta-gamma de-correlations were anatomically segregated from those LFP pairs showing increased theta-gamma correlations.

Taken together, these results suggest that LFP pairs showing a reduced cross frequency correlation after the attention cue onset may constitute a phenomenon that relates to a de-coupling of local brain circuits that are not engaged in actual attentional stimulus selection."

Result A4 - Relation of cross-frequency correlations to LFP power modulation at theta and gamma frequency bands.

I tested for a relationship between theta-gamma correlation and overall power modulation after observing apparent theta band peaks in the power spectra but no overall gamma band peak across theta-gamma P-A correlated channels (**A1** Fig S5). Of the LFP pairs with significant theta - gamma correlations 73% (50/74) of the unique phase-modulating LFPs showed theta (4-9) Hz peaks of individual power spectra. The difference in MI from pre- to post- attention cue did not correlate with the change in overall power in either the phase-providing, or the amplitude-providing LFPs which showed significant P-A correlations after the attention cue. However, in

the gamma-amplitude providing LFPs in these LFP pairs, the strength of post-cue MI correlated with gamma power on correct trials (at 40 Hz, r = 0.22, p=0.0.048; Spearman rank correlation).

Result A5 - Relation of the gamma amplitude variations to the time of cue onset versus the phase of remote theta band fluctuations.

I validated that the high frequency gamma amplitude more precisely locked to the theta-band phase of a distant recording sites than to the time of attention cue onset. If gamma amplitudes lock more precisely to cue onset, then this would suggest that the cross-frequency correlation effect is secondary to a cue-triggered gamma response at some neuronal recording site (Aru et al., 2015). I evaluated this scenario by quantifying 1) the variance across trials of the time difference between cue onset and the time of the maximum amplitude of the high frequency gamma component and 2) the jitter (variance) of the phase of the theta frequency component at the time of the maximum amplitude of the high frequency gamma component. Finally I compared the two types of variance of the gamma amplitude across LFP-LFP pairs. The gamma amplitudes were more precisely locked (i.e. showed less variance) to the phase of the theta band modulation than to the attention cue onset. On average across the 85 LFP pairs that showed significant P-A correlation, 90.6 % of LFP pairs showed maximum gamma amplitudes that were more precisely locked to theta phase than to cue onset (**Fig. A3C**). This finding supports the conclusion that the gamma LFP events were tightly linked to the theta phases measured at distant electrodes, rather than constituting statistically independent or only spuriously linked events.

Result A6 - Equalizing the number of correct and error trials using a randomization approach.

I ran a shuffling procedure with 1000 surrogates and recalculated the normalized difference in MI for theta-gamma correlation using the same number of correct trials as error trials to determine any trial-number related bias in cross frequency correlation.

I first quantified the population level comparison of error and correct theta-gamma correlations (across the 84 of 85 LFP pairs that had more trials in correct than error trials) for each surrogate of correct trials against the observed error MI values (1000 Wilcoxon one-tailed signrank tests in total). Tthe difference in pre-to-post cue change in theta-gamma correlation on correct trials was significantly ($p < 0.05$) higher than the corresponding change in error trials in 968/1000 (96.8%) of surrogates. In other words, the increase in P-A correlation found on correct, but not error trials is highly reliable when controlling for the number of trials. Moreover, I quantified for each LFP pair how often correct shuffled MIs were higher than the observed error MIs when equating the number of trials. On average across LFP pairs 64% ± 3.1 SE of correct shuffled MIs were higher than the observed error MIs.

I next corroborated the phase preference evident during theta-gamma correlation on correct trials after equalizing for the number of error trials. To this end, I took the average phase for individual LFP pairs, and calculated the preferred phase as before. The distribution of preferred phases of the trial-equated shuffled amplitude distributions (mean phase of -14.03^0, 95% CI $[-40.26^0, 12.20^0]$) was the same as the observed amplitude distribution, deviated from uniformity (Hodjes-Ajne test, $p=0.00036$), and was dissimilar to the error amplitude distribution (Kuiper test, $p<0.005$).

Result A7 - Accounting for differences of overall modulation strength of correct and error trials on phase preference

The main text describes the preferred phase analysis based on the modulation index. I repeated the phase analysis with another metric that weights the low frequency phase alignment of high frequency activity by overall modulation strength (van der Meij et al., 2012). The phase analysis of the weighted phase locking factor (wPLF) confirmed that correct and error phase distributions were significantly different from each other (**Table A1**). In addition, this analysis also showed that error trials were not associated with a statistically reliably preferred phase across LFP channels (**Table A1**). In contrast, the wPLF analysis confirmed that correct trials showed a non-uniform, preferred mean phase for theta-gamma correlation (**Table A1**). Control analysis of the peaks of the amplitude distribution also confirmed a statistically significant preferred phase of theta gamma correlation on correct but not error trials, and a significant difference between correct and error distributions (**Table A1**). Together with the results in **Result A6** above, correct trials were characterized by high frequency gamma band activity that correlated with reliably similar phases across pairs of LFPs engaging in theta-gamma correlation.

Result A8 - Testing for the effect of the average field potential to explain the difference of P-A correlation in correct versus error trials.

I observed a peri-cue average LFP potential that was an evoked field from the stimulus color onset preceding the attention cue onset. I tested whether this non-stationary peri-cue event influenced the post-cue enhanced theta-gamma correlation effect (Aru et al., 2015) using a cluster-based permutation test (Maris and Oostenveld, 2007). No significant temporal clusters emerged ($p>0.05$). In other words, the average field was not different on correct versus error

trials for those LFPs that provided the phases or the amplitudes of the theta-gamma correlated LFP pairs.

Result A9 - Testing global distribution of phase or amplitude LFPs

Despite the fact that all subareas contained phase and amplitude providing LFPs engaging in theta-gamma correlation (**Figure 4B,C**), the relative proportion of all theta-gamma P-A correlated LFP pairs across VMPFC, ACC, and lateral PFC was not significantly different than expected by chance (**Figure 4C**; χ^2 test with Yates correction, χ^2 =9.67, p=0.65). Moreover, the relative proportion of inter-areal phase- and amplitude- providing LFPs showed a trend but was not different significantly from a uniform distribution (**Figure 4D**; χ^2-test, χ^2 =5.4, p=0.067 and χ^2 =4.93, p=0.085, phase- and amplitude- providing LFPs, respectively).

Result A10 - The relation of phase synchronization, phase resetting, and phase-amplitude correlation

Gamma amplitude modulation, and thus theta-gamma P-A correlation, in a target region may be the result of bi-directional theta-phase synchronization across regions. One possibility is that there is a large-scale phase reset across ACC/PFC subfields, which would align oscillations and result in large-scale theta phase synchrony. However, the theta phase reset is rather localized to the nexus of VMPFC, ACC and lateral PFC (**Fig. 6**), which rather suggests that theta phase synchronization may not necessarily spread across all ACC/PFC fields that show significant theta-gamma correlations. To address these considerations, I analyzed phase synchronization in the same LFP pairs that showed significant theta-gamma P-A correlation in order to describe the interaction between phase synchronization, phase-amplitude correlation, and phase resetting.

Note that the LFP pairs used in this analysis were exactly the same LFP pairs used to calculate the phase and amplitude correlation.

First, I quantified phase synchronization (using the weighted phase lag index, wPLI), defined its temporal specificity, and determined its functional relevance. This measure removes artifactual coherence from volume conduction. There was significant phase synchronization in the 4-7 Hz range and the 17-34 Hz range on correct trials in both the pre- and post-cue epochs (**Fig. A6**A, Wilcoxon signrank test, $p<0.05$ for both, correct and error trials, FDR corrected). On error trials, peak phase coupling shifted from 25 Hz in the pre-cue period to 21.5 Hz in the post-cue period (**Fig. A6**B, Wilcoxon signrank test, $p<0.05$ for both, correct and error trials, FDR corrected). Furthermore, there was no significant change in phase synchronization after attention cue onset at any of the frequencies considered (Wilcoxon signrank test for paired samples, $p>0.05$, FDR corrected).

Because I wanted to compare theta phase synchronization with theta-gamma phase-amplitude correlation, I restricted further analysis to the theta frequency phase. The wPLI did not significantly differ between correct and error trials in either the pre- or post-cue epochs (Wilcoxon sign rank test for paired samples, $p>0.05$), suggesting that in the network of LFP pairs , theta phase synchronization does not predict behavioural outcome.

I next determined the link between the cross-frequency P-A correlation and phase synchronization. I limited this correlation analysis to correct trials because both measures showed significant phase synchronization and theta-gamma correlations on these trials. There was a weakly negative, but significant correlation of the wPLI in the post-cue epoch with theta gamma P-A correlations (Spearman rank correlation, $r=-0.22$, $p=0.048$). To test whether phase synchronization tended to decrease when phase-amplitude correlation increases, I compared the

change in phase synchronization with the change in phase-amplitude correlation from pre- to post-cue, but found no correlation (Spearman rank correlation, R=0.067, p=0.54).

Finally, I tested for a possible link between phase synchronization and the phase reset . I correlated the phase synchronization in the pre-cue period and the post-cue period. In line with the conclusion that phase synchronization did not change in time, there was a positive correlation with slope 1 (**Fig. A6C**). I highlighted the LFP pairs where the phase channel showed a significant phase reset in the 150-250 (± 50) ms after attention cue onset in the previous analysis. Notably, the highlighted phase resetting LFPs are broadly distributed among those LFP pairs that showed either weak or strong phase synchronization.

In summary, the observed theta-gamma P-A correlation does not apparently relate to LFP-LFP theta band phase synchronization. Phase synchronization neither tracks attention cue onset, nor indexes the behavioural outcome. Moreover, the negative correlation with theta-gamma P-A correlation suggests that the two phenomena may be involved in different processes. In support of this, significant phase resets (associated with phase-amplitude correlation, but not phase coupling) occurred even when the network showed weak phase coupling.

Result A11 - Selectivity of theta-gamma correlation for the attended target location or reward outcome associated with the target location

To quantify whether theta-gamma P-A correlations carried information about the location of the attentional target stimulus and about the reward outcome associated with the attended target stimulus, we I performed two types of analysis (see Methods for details). First, we I conducted a population level analysis to discern the overall selectivity across LFP pairs.

Secondly, we I applied single LFP-pair statistics to infer how often selectivity is reliably (statistically significant) evident across trials of single LFP pairs.

11.1. Selectivity for spatial target location of attention.

First, at the population level, there was a trend for higher increases in theta-gamma correlation when attention was cued contra-laterally versus ipsi-laterally (**Fig. A7A, left panel**; Wilcoxon sign rank test, $p=0.066$). This statistical trend suggests that individual LFP pairs may carry significant spatial attention information in theta-gamma P-A correlation. I thus determined in a second step if individual pairs showed a significant preference for the contra- or ipsilateral attention conditions. There were 49 of 1104 (4.4%) LFP pairs with a preference for a specific spatial location (Monte Carlo surrogate test, two-sided, $p<0.05$). Among those 49 LFP pairs, n=32 (65%) showed stronger theta-gamma correlation when attention shifted to a contralateral stimulus, whereas n=17 (35%) showed stronger theta-gamma correlation for ipsilateral attention.

Among the theta-gamma correlated subnetwork (i.e. the n=85 LFP pairs that showed significant theta-gamma correlation on correct trials), there was no statistically reliable, average difference in theta-gamma correlation between contra- and ipsilateral attention (**Fig. A7B, left panel;** Wilcoxon sign rank, $p=0.14$). Considering the single LFP pair statistics, 5 of the 85 individual LFP pairs showed a significant preference for spatial allocation, as evidenced by the differential change in theta-gamma correlation between conditions Monte Carlo surrogate test, $p<0.05$). In summary, these results document that theta-gamma correlation at the single LFP-pair encodes spatially specific attention information in a small subset of LFP pairs (4.4%), but that a larger proportion of LFP pairs engage in theta-gamma correlation without apparent, single LFP pair level selectivity for the spatial hemifield of the attentional target stimulus.

11.2. Selectivity for the reward outcome associated with the attended target stimulus.

In the majority of experimental sessions, the reward outcome associated with the cued attentional target stimulus was manipulated by associating the color of the stimulus to higher or lower reward magnitude (*see* **A1 Methods**). This reward outcome association was not instrumental for solving the task (attention had to be shifted to the cued location irrespective of the associated reward magnitude), but it could influence the LFP activity during the attention shift period, similar to its influence on the firing rate of a subset of neurons (*see* (Kaping et al., 2011)).

To test for this, we I calculated theta-gamma phase-amplitude correlations for trials where the cued target was associated with higher or lower associated reward outcome. Among 860 LFP pairs recorded in sessions with reward outcome manipulations, there was on average no difference in the change of the theta-gamma correlations when attention shifted to a higher or lower rewarded attentional target stimulus (**Fig. A7A, right panel**; Wilcoxon sign rank test, $p=0.40$). At the level of the individual LFP pairs, 45 of 860 (5.2%) LFP pairs showed a statistically significant difference in theta-gamma phase-amplitude correlation for high vs low targets (Monte Carlo surrogate test, $p<0.05$), with 21 (47%) and 24 (53%) showing a greater increase on trials with attention to a lower and higher rewarded target, respectively.

These results were largely preserved when analyzed separately for those LFP pairs that showed a post-cue increase in theta-gamma correlation irrespective of attention condition and which were recorded in experimental session with a reward outcome difference between attentional targets (n=68 of the 85). The change in theta-gamma correlation was not different between higher vs. lower reward outcome conditions (**Fig. A7B, right panel;** Wilcoxon sign rank, $p=0.78$). Only one of these 68 LFP pairs showed a statistically reliable difference in the

theta-gamma correlation between higher vs. lower reward outcome conditions (Monte Carlo surrogate test, $p<0.05$). In summary, these results illustrate that a small subset of single LFP-pairs engages in theta-gamma correlation significantly stronger when attention is deployed to a high (vs. low) rewarded attentional target, and a similarly small subset engages in significantly stronger theta-gamma correlation with attention to a lower (vs. higher) rewarded attentional target. Consistent with this result, there was no preference for higher or lower rewarded targets at the grand average population level.

Taken together, these results show that for subsets of recorded LFP pairs the strength of theta-gamma correlation provides statistically reliable information about task-relevant variables. This finding calls upon future studies to test specifically how theta-gamma correlation contributes to the encoding of task relevant variables. These more specific tests may explicitly focus on those LFP recording sites in which variations in the LFP phase, or the LFP amplitude carry already specific information about task relevant variables about, e.g. the location or expected reward magnitude. One possible result of these future analysis maybe that theta-gamma phase amplitude correlation does emerge particularly for pairs of LFP recording sites that encode separable types of task relevant information (including stimulus features and their spatial location, reward expectancies, or rule-based stimulus response rapping rules) that is integrated or gated through theta-gamma correlation (Lisman and Jensen, 2013).

APPENDIX B: FIGURES & TABLES

Figures and Tables for Main Results

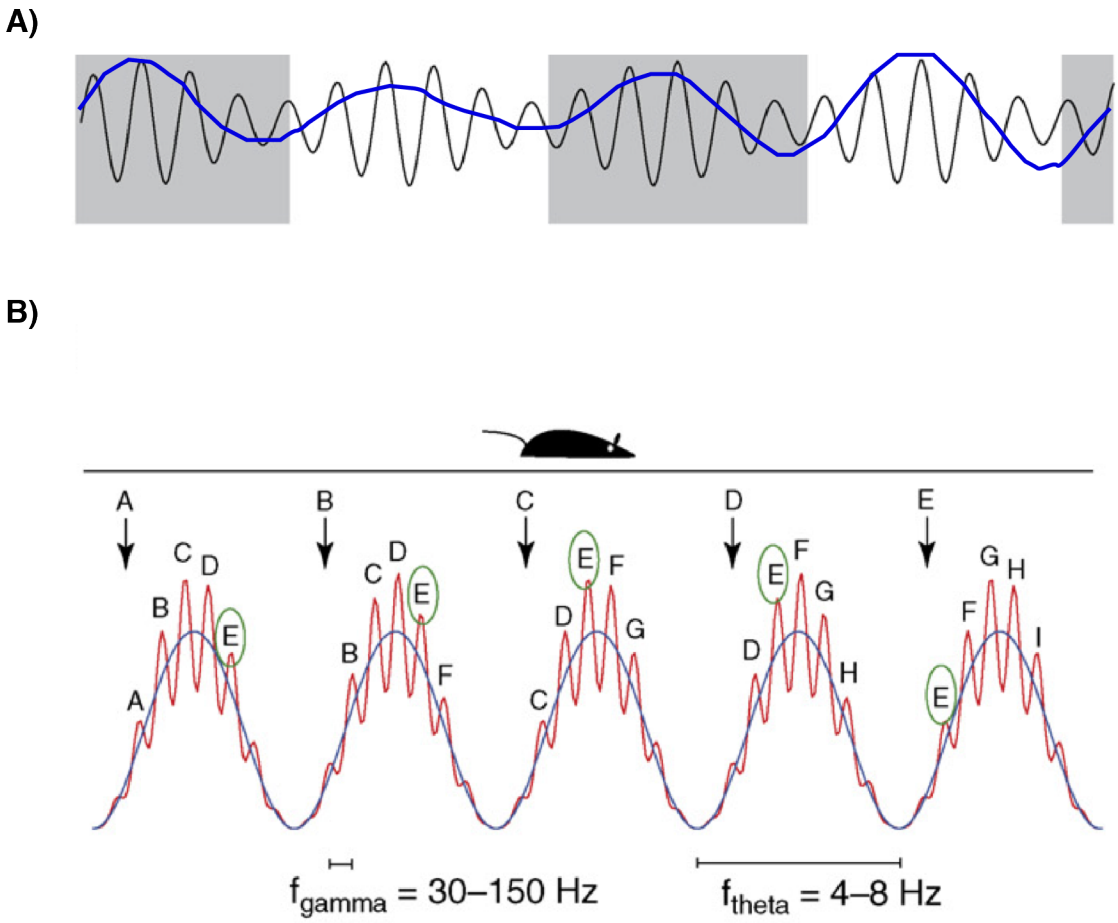

Figure 1. Phase-amplitude interactions support phase precession
(A) Illustration of phase-amplitude correlation for a faster gamma oscillation (black line) and a slower theta oscillation (blue line). Notice that gamma amplitude waxes and wanes in direct relation to the phase of the ongoing theta rhythm, but is not related to the amplitude of theta.
(B) Illustration of phase precession in rodents. As the rodent moves through its environment, place cells representing its position are activated. Neural ensembles encoding location are represented in gamma (red line). As the rat advances, place cells are activated earlier in the theta-cycle (blue line), with a corresponding change in the amplitude of gamma frequency. Different ensemble are read out in relation to the phase of theta, suggesting an ordered, compressed read out of upcoming position. Notice that the amplitude of gamma is directly related to the phase of an ongoing theta rhythm. Adapted from (Jensen and Colgin, 2007).

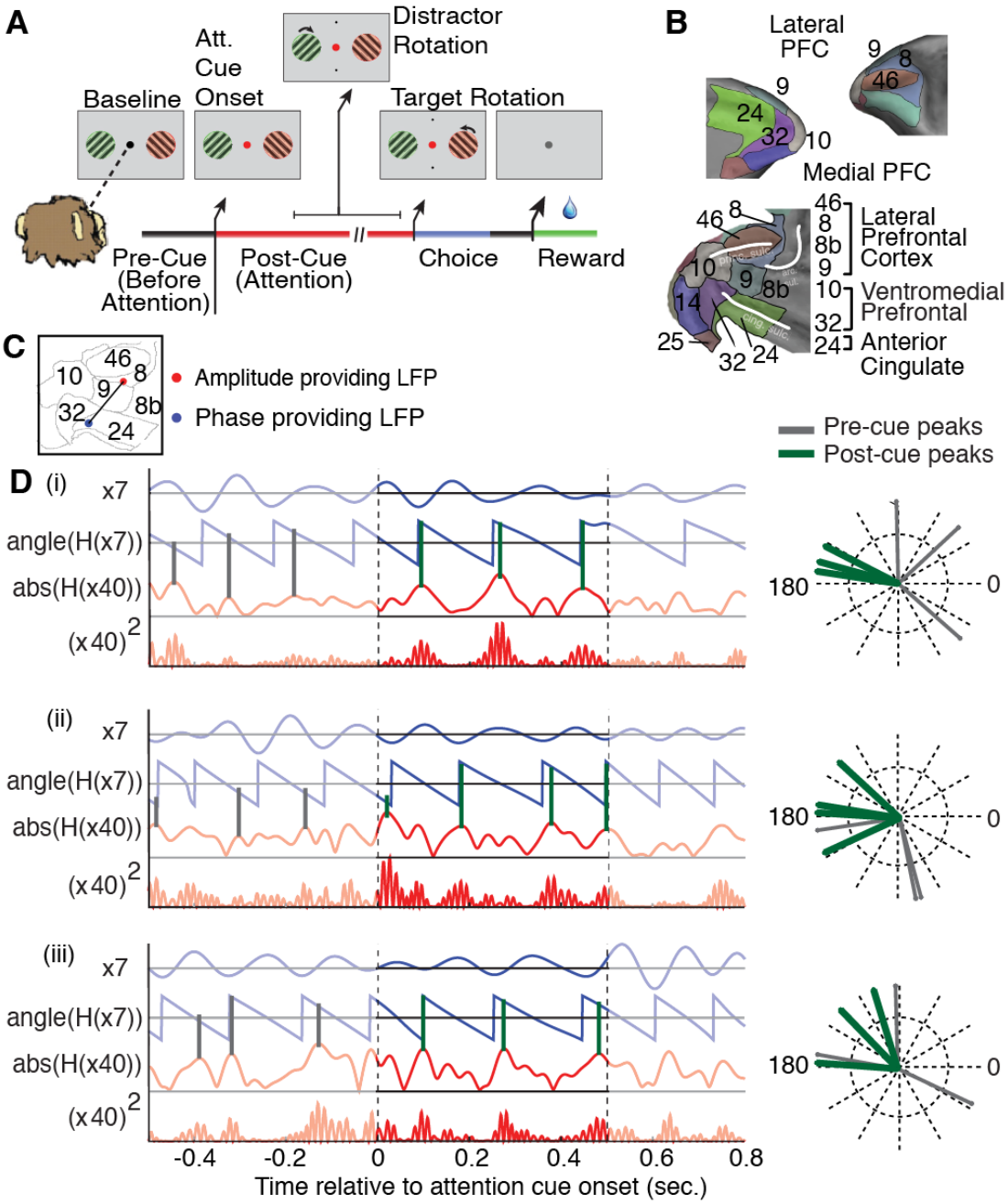
A
Distractor Rotation
Att. Cue Onset
Baseline
Target Rotation
Pre-Cue (Before Attention)
Post-Cue (Attention)
Choice
Reward
B
Lateral PFC
Medial PFC
Lateral Prefrontal Cortex
Ventromedial Prefrontal
Anterior Cingulate
C
Amplitude providing LFP
Phase providing LFP
Pre-cue peaks
Post-cue peaks
D
(i)
(ii)
(iii)
x7
angle(H(x7))
abs(H(x40))
(x40)2
180
0
-0.4
-0.2
0
0.2
0.4
0.6
0.8
Time relative to attention cue onset (sec.)

Figure 2. Task and illustration of example theta-gamma correlation
(A) The selective attention task required monkeys to keep fixation on a central cue throughout a trial, while presented with two peripheral grating stimuli. First, both grating stimuli changed their color simultaneously to either green or red, the location of which was random. Then, the fixation point changed its colour to match the stimulus to which the monkey has to covertly shift attention. The attended stimulus rotated transiently at unpredictable times, requiring the monkey to judge a clockwise/counterclockwise rotation to receive fluid reward. Rotations of the non-attended stimulus had to be ignored (filtered).
(B) Lateral and medial prefrontal cortex of macaques rendered in 3D (*upper panels*) and represented as 2D flat map (*bottom panel*) with a standard labeling of cortical fields (for details, *see* **Fig. A1**).
(C) Anatomical locations on the 2D flat map of an example LFP pair in which the LFP theta phase of one recording site in the ACC (blue dot) correlated with the low-gamma amplitude of a second LFP recording site in lateral PFC area 8 (red dot).
(D) Filtered phase and amplitude traces for the example LFP-LFP pair that is shown in **(C)** for three correct trials **(i-iii)**. For each trial, the bandpass filtered low frequency activation and its phase evolution is shown with blue lines, and the amplitude envelope and the squared gamma amplitude of the amplitude providing LFP recording is shown in red. Grey (green) vertical lines highlight the phases at which the gamma amplitude variations show peaks within the 500 ms before (after) attention cue onset. The polar plot on the right shows these peak phases in the pre- and post-cue epoch. For this ACC - LPFC example pair, the gamma amplitude peaks of the PFC channel correlate with similar theta phases of the ACC channel in the post-cue period. For more examples *see* **Fig. A2**.

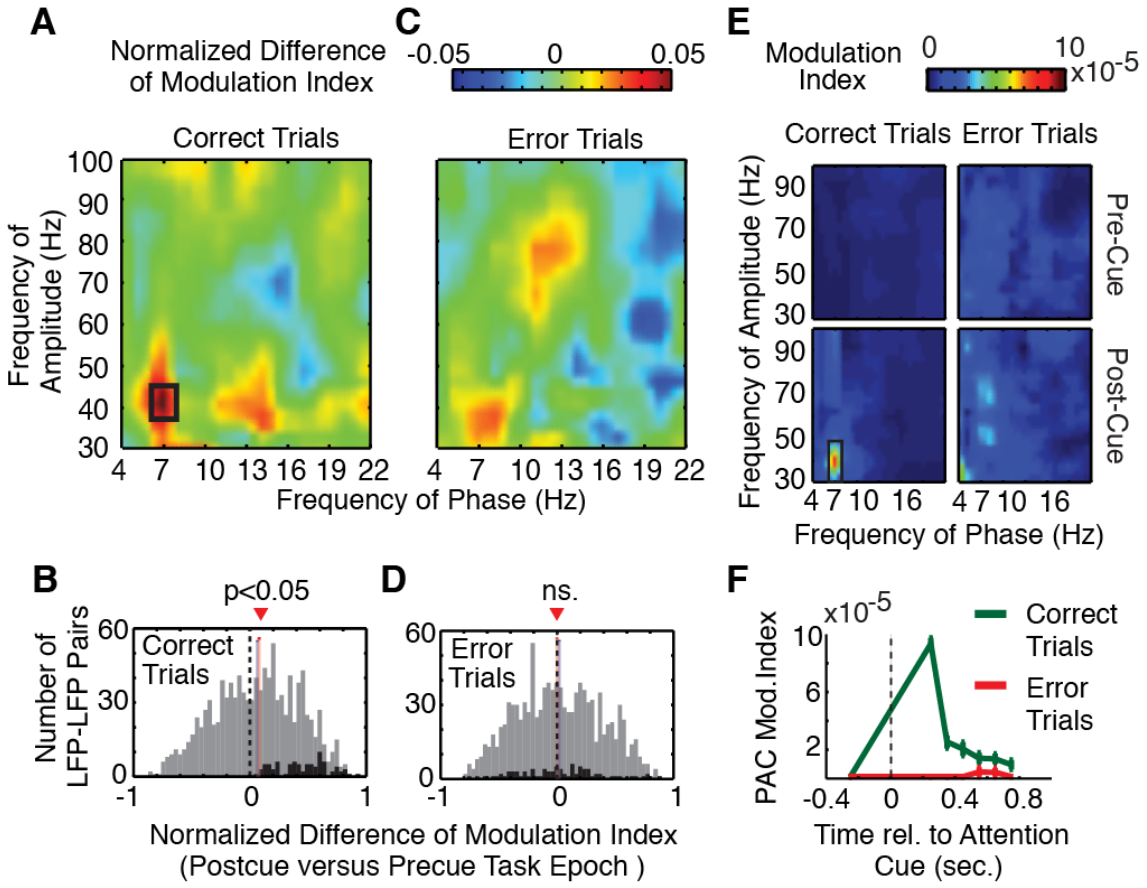

Figure 3. Theta-gamma correlation is significantly enhanced after attention cue onset on correct trials

(A) Comodulograms of the normalized difference in the Phase (*x-axis*) - to - Amplitude (*y-axis*) correlation (measured as MI) in the post-cue relative to the pre-cue task epoch on correct trials across LFP pairs (n=1104). Each LFP pair was normalized indepdently (see Methods). Positive values indicate increases of P-A correlation after attention cue onset. The black rectangle denotes significant ($p < 0.05$) co-modulation difference.

(B) Histogram of the difference in theta-gamma P-A correlation Modulation Index in the post-cue relative to pre-cue task epoch across all LFP-LFP pairs on correct trials (n=1104). Black bars in both panels highlight those LFP pairs that exhibited an individually significant P-A correlation increase with attention on *correct* trials (n=85). Red and blue vertical bars denote mean and median of the distribution, and the dotted line highlights the difference in MI of zero.

(**C**,**D**) Same format as **(A,B)** but for error trials. Note that in (**D**) the black bars in the histogram show the theta-gamma MI values for the *same* LFP pairs highlighted in **(B)**.

(E) Comodulograms showing the average P-A modulation index on correct trials (*left column*) and error trials (*right column*), and in the pre-cue task epoch (*upper row*) and the post-cue epoch (*bottom row*) (n=85). Shown are the average MI's of those LFP-LFP pairs with significantly increased theta to gamma P-A correlation (the black colored bars in **(B)**).

(F) Temporal evolution of theta-gamma P-A correlation for those LFP pairs with a significant P-A correlation effect on correct trials (n=85) during correct (green) and error (red) trials at

different 500 ms time windows relative to the attention cue onset (*x-axis*).

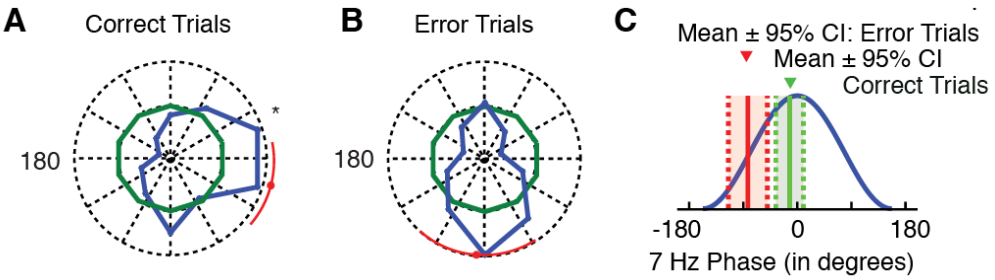

Figure 4. Preferred theta phase of theta-gamma correlation on correct and error trials
(A) Polar histogram of the amplitude-weighted mean preferred phases in the post-cue period at which gamma activity phase locked in those LFP pairs with significant theta-gamma coupling in the post-cue period (n=85). Colors denote the distributions expected by chance (*green*) and from the post- attention cue epoch (*blue*) on correct trials. The outer dotted ring corresponds to a proportion of 20%. The red dot and line denote circular mean and 95% confidence range.
(B) Same as in **(A)**, but for error trials.
(C) Illustration of the mean and 95% confidence range of the preferred theta phases on correct (green) and error trials (red) at which gamma amplitudes couple for the LFP pairs that showed a significant increase in theta-gamma P-A correlation after attention cue onset.

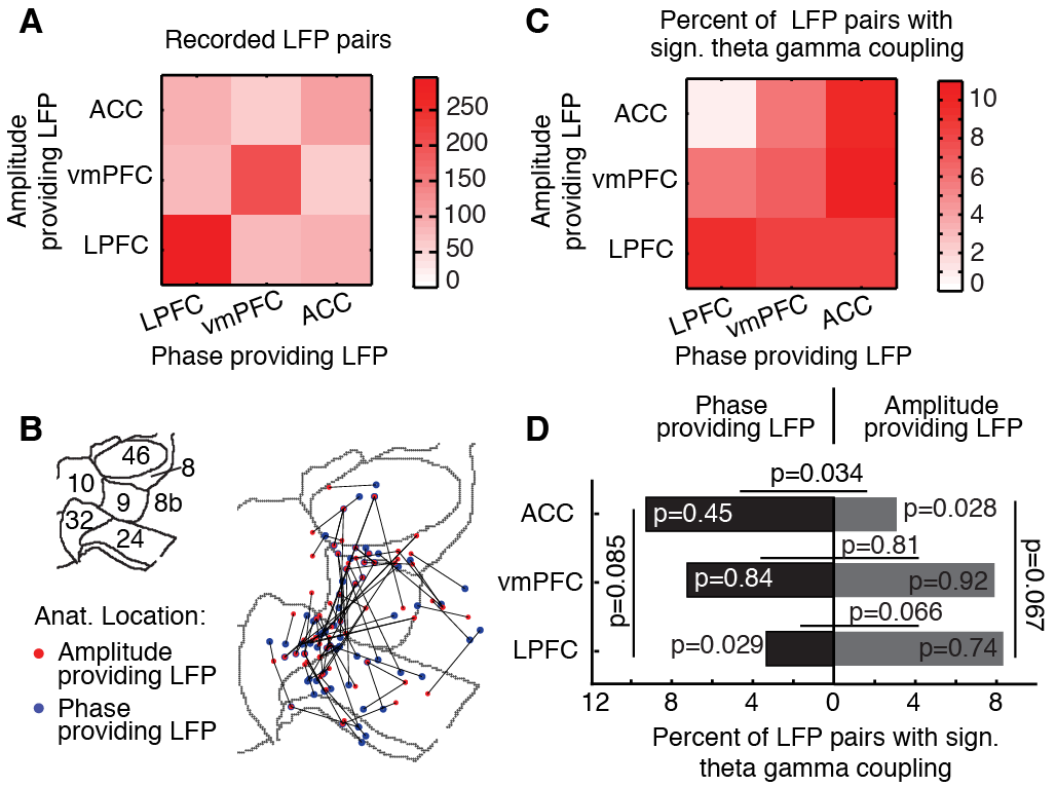

Figure 5. Anatomical origins of cortical sites with phase and amplitude modulation during theta-gamma correlation

(A) Combination matrix showing the total number of LFP-LFP pairs (n=1104) recorded from the ventromedial PFC (VMPFC, area 32 and 10), the anterior cingulate cortex (ACC, area 24), and the lateral prefrontal cortices (areas 46, 8, and 9). The brain area of the phase providing channels is on the *x-axis*, and the origin of the amplitude providing LFP channels is on the *y-axis*.

(B) Anatomical recording location of phase- (blue) and amplitude- (red) providing LFPs (n=85 LFP pairs; connected with black lines) and plotted on the 2D flatmap representation of the ACC and PFC. Grey contours denote area boundaries (*see* inset for area labels; **Fig. 2B**).

(C) Same as in **(A)**, but for the proportion of theta-gamma P-A correlated LFP pairs (n=85) relative to all LFP pairs recorded for an area combination. Color indexes the proportion.

(D) Likelihood to find a phase providing channel (values left from zero) and an amplitude providing channel (right from zero) in the VMPFC, ACC, and lateral PFC during cross-area theta-gamma correlation (n=32; *y-axis*).

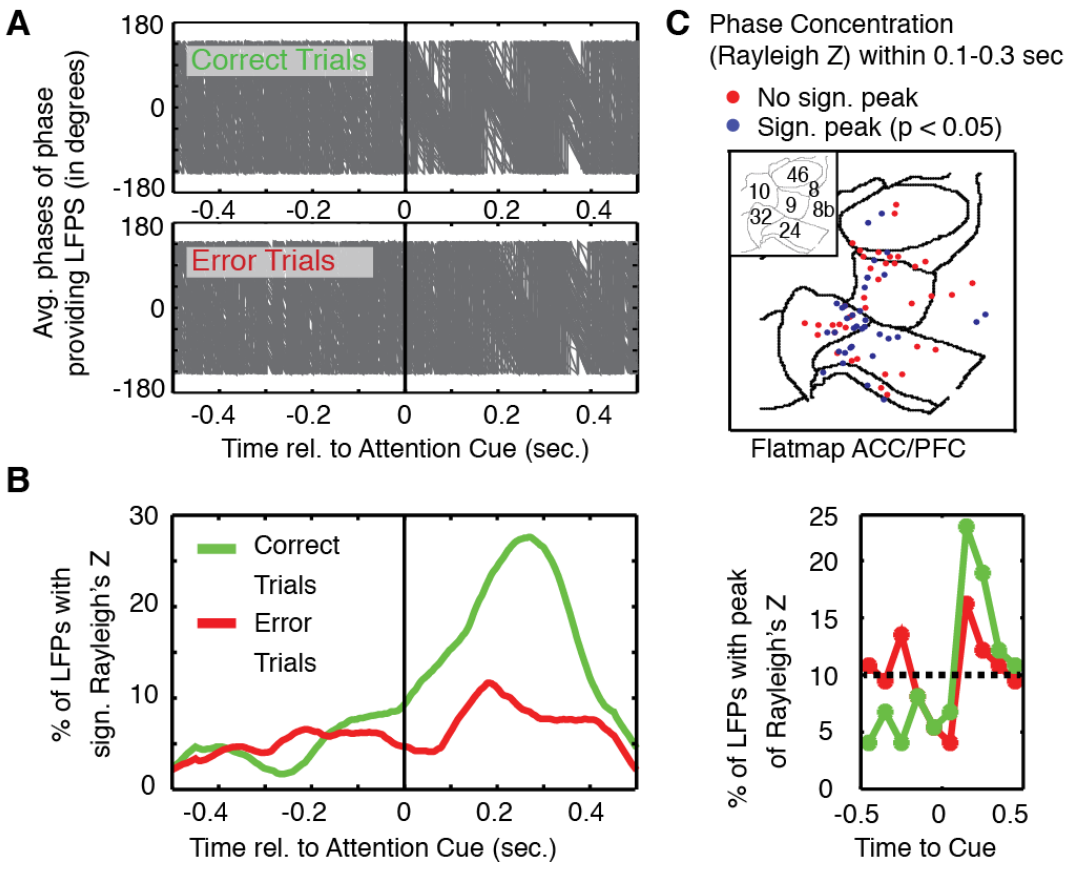

Figure 6. Phase providing LFPs engaging in significant theta-gamma correlation show a theta phase reset after attention cue onset on correct trials

(A) Progression of the average phase (*y-axis*) for all phase-providing LFP channels (n=74) engaging in significant theta-gamma correlation around the time of the attention cue onset (*x-axis*). Each grey line represents the average phase across trials of one such LFP. Top- and bottom- panels show the progression of mean phases on correct trials and on error trials, respectively.

(B) The left panel shows the percentage of phase-providing channels with significant phase concentration (*y-axis*, measured as Rayleigh's Z) around the time of the attention cue onset (*x-axis*). Green and red lines show the average Rayleigh's Z across LFP channels for correct and for error trials, respectively. The panel on the right shows the percentage of LFPs whose peak phase concentration fell within one of 10 non-overlapping time bins (around attention cue onset).

(C) The anatomical distribution of recorded LFPs that showed a significant phase concentration (blue) or that did not show significant phase concentration (red) in the 100-300 ms. following attention cue onset. See **Fig. 2B** for the labeling of PFC / ACC brain areas on the 2D flatmap representation (and **Fig. 2** and **2**).

Table 1. The relationship of theta gamma phase amplitude correlation and burst-LFP synchronization across all types of channel combinations

The table shows the Spearman-Rank correlations and their respective significance levels. ***Columns*** are split into the theta phase providing channels and the gamma amplitude providing channels. Different columns show either all channels, *or* channels from LFP pairs that showed significantly increased phase amplitude correlation in the post cue period. ***Rows*** show the results separately for channels at which either the LFP (upper 3 rows) or the burst firing of neurons (lower 3 rows) were part of a burst-LFP pairs.

For recording channels with more than one single cell, the average burst-LFP synchronization across cells for that channel was used for calculating the correlation. Values in red font denote positive correlations at $p < 0.05$, blue font denotes negative correlations at $p < 0.05$, and values in bold black font highlight correlations >0.1. Boxes with significant ($p<0.05$) correlation are highlighted in a black box.

		Theta-Phase providing LFP channels		**Gamma-Amp.** providing LFP channels	
		All	Those with sign. Theta-gamma correlation	All	Those with sign. Theta-gamma correlation
'LFP Channel' of burst-LFP synchronization pair; LFP recorded at the same channel as used for the cross-frequency analysis	**Theta (5-10Hz)** Burst-LFP synchronization	p=0.261, r=0.036	p=0.713, r=0.038	**p=0.027, r=0.072**	p=0.702, r=0.040
	Beta (15-25Hz) Burst-LFP synchronization	p=0.155, r=-0.046	**p=0.016, r= -0.246**	p=0.086, r=0.056	**p=0.032, r= -0.219**
	Gamma (55-75Hz) Burst-LFP synchronization	p=0.069, r=0.059	p=0.701, r=-0.040	p=0.138, r=0.048	p=0.163, **r=0.143**
'Burst Channel' of burst-LFP synchronization pair; Burst Firing of neurons at the same channel as used for the cross-frequency analysis	**Theta (5-10Hz)** Burst-LFP synchronization	p=0.728, r=0.010	p=0.255, **r=0.114**	p=0.657, r=0.013	p=0.266, **r=0.111**
	Beta (15-25Hz) Burst-LFP synchronization	p=0.482, r=0.021	p=0.406, r=0.083	p=0.581, r=-0.017	p=0.234, **r=0.119**
	Gamma (55-75Hz) Burst-LFP synchronization	p=0.070, r=0.055	**p=0.044, r=0.200**	p=0.750, r=0.010	p=0.476, r=0.071

Figures and Tables for Supplementary Results

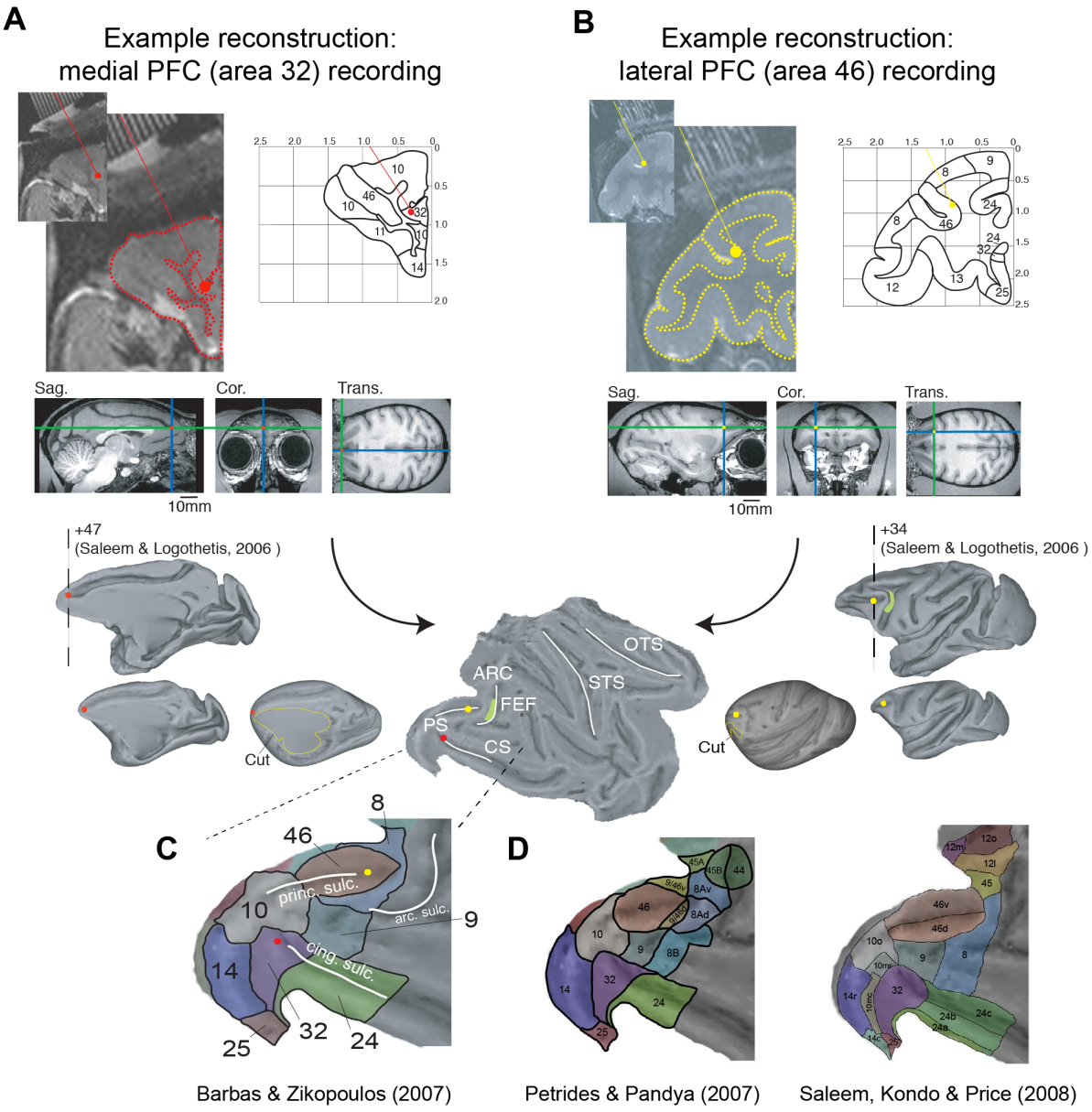

Figure A1. Illustration of anatomical reconstruction of recording sites
(**A**, **B**) Reconstruction of a medial PFC (area 32, **A**), and a lateral PFC (area 46, **B**) recording site started from the 7T anatomical MR, which was obtained with (iodine based) visualization of electrode trajectories within the electrode grid placed inside the recording chamber. The outline of the cortical folding was sketched on the coronal MR slice to ease identification of areas and landmarks according to standard brain atlases, and to place the depth of the electrode tip (red dot in **A** and yellow dot in **B**) with custom MATLAB code. The electrode tip position was then placed into a standardized macaque brain available in the MR Caret software package. Caret allowed rendering the MR slice into a 3D volume and to inflate the volume before the spherically inflated brain was cut (indicated as yellow line) to represent it as 2D flat map. White lines on the flat map demarcate the principal sulcus (PS), the arcuate sulcus (ARC), and the cingulate sulcus (CS). The location of the FEF (frontal eye field) within the ARC is indicated by a green patch.
(**C**) As a last step, the anatomical subdivision of areas in the prefrontal-cingulate cortex were visualized following the nomenclature from (Barbas and Zikopoulos, 2007). The area 32 and area 46 recording sites are visualized throughout the panels by a red and a yellow dot, respectively. (**D**) Similar format to (**C**), but using major anatomical reference schema (Petrides and Pandya, 2007; Saleem et al., 2008). Adapted from (Kaping et al., 2011).

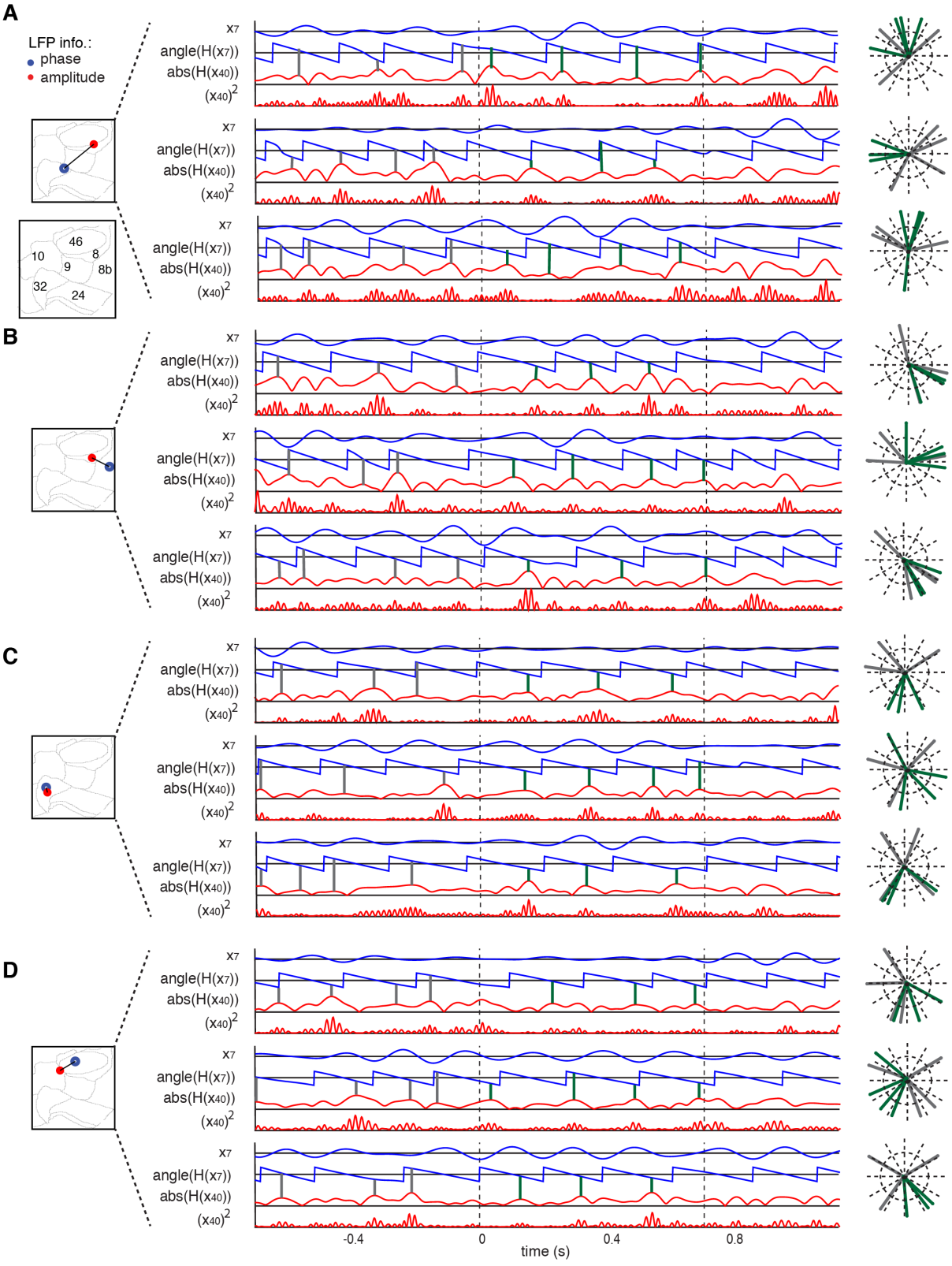
A
B
C
D
LFP info.:
phase
amplitude
46
8
10
9
8b
32
24
x7
angle(H(x7))
abs(H(x40))
(x40)2
-0.4
0
0.4
0.8
time (s)

Figure A2. Example LFP-LFP pairs showing theta-gamma correlation in the post-cue period

(**A-D**) Example LFP-LFP pairs shown in same format as Figure 2D in the main text. Filtered phases and amplitude traces for the example LFP-LFP pairs that are shown in insets of the 2D ACC/PFC representation. For each of three trials (i-iii) the bandpass filtered low frequency activation and its phase evolution is shown with blue lines, and the amplitude envelope and the squared gamma amplitude of the amplitude providing LFP recording is shown in red. Grey (green) vertical lines highlight the phases at which the gamma amplitude variations show peaks within the 500 ms before (after) attention cue onset. The polar plot on the right shows these peak phases in the pre- and post-cue period. For all example LFP-LFP pairs, the gamma amplitude peaks in the 500 ms time after cue onset couple to similar theta phases of the phase channels in the post-cue period across trials.

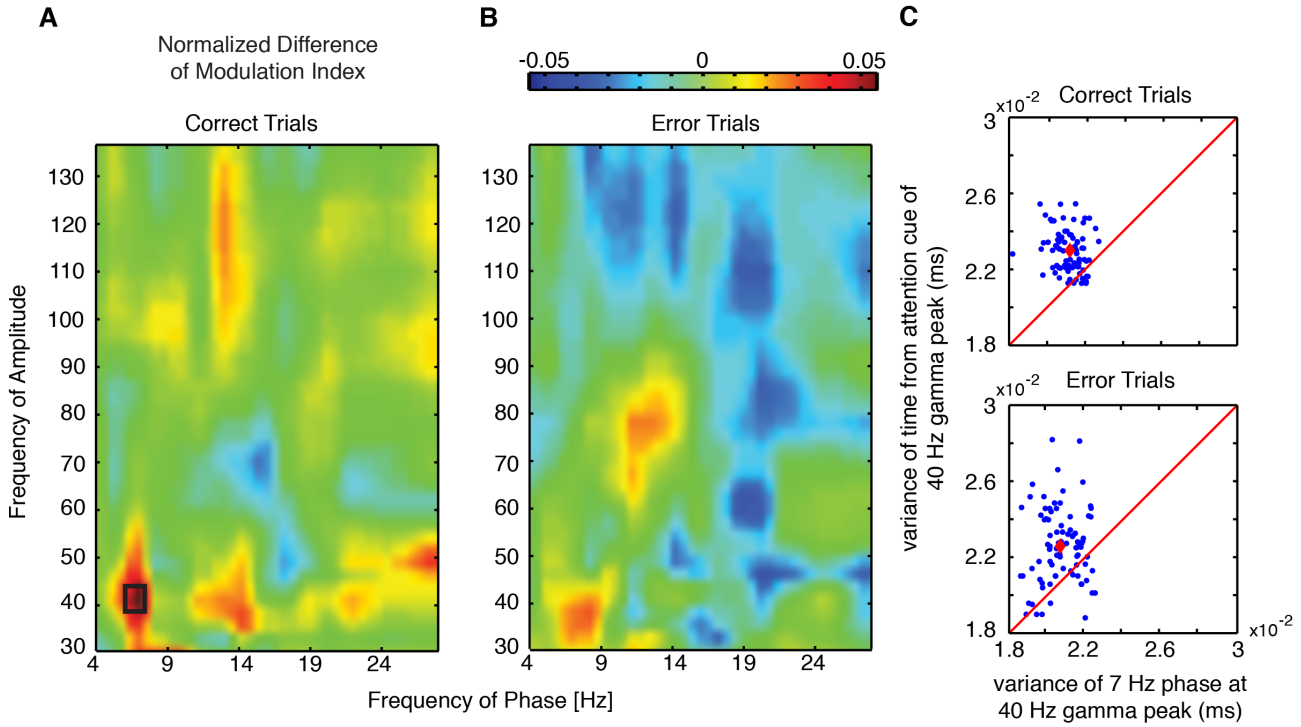

Figure A3. Theta-gamma correlation is significantly enhanced after attention cue onset on correct trials in a narrow theta-gamma range

(**A** and **B**) Same format as **Fig. 3A,B** in the main text. Comodulograms of the normalized difference in the Phase (*x-axis*) - to - Amplitude (*y-axis*) Correlation (measured as MI) in the post-cue relative to the pre-cue task epoch (n=1104). Positive values indicate increases of P-A correlation after attention cue onset. The *left* and *right panels* shows PAC difference for correct and error trials respectively. The black rectangle denotes significant ($p<0.05$, FDR corrected) co-modulation difference.

(**C**) Scatter plot of the variance of the time from attention-cue onset (*y-axis*) and circular variance of the phase (x-*axis*) relative to the maximum peak of the gamma envelope (n=85). The red line denotes where variances are equal, and the red dot is defined by the average variance. .

Table A1. The distribution of preferred phases of coupling is significantly non-uniform for correct but not error trials

The average (±confidence intervals) of preferred phases are shown for correct trials and error trials. Reported are p-values associated with either the Hodjes-Ajne test for circular non-uniformity (n=85, each), or the Kuiper test for the difference between 2 sample distributions. Bolded values are significant at $p<0.05$. Different methods of analyzing the distribution of phases to which gamma activity coupled agree that correct trials are non-uniform, while error trials are not. Moreover, 2 different metrics (MI and wPLF) agree that the two distributions are different from one another.

			Method of Phase Extraction					
Statistical Test	Null hypothesis		MI	wPLF	$Peaks_{max}$	$Peaks_{80}$	$Peaks_{70}$	$Peaks_{50}$
Hodjes-Ajne test	**Correct trials:** the distribution of phases is non-uniform	Mean ± 95% CI Phase (deg)	-14.7 ± 26.3	9.0 ±27.2	-8.1 ±69.7	-1.6 ±51.2	1.0 ±46.8	-6.7 ±37.9
		p-value	**0.00036**	**0.00088**	**0.0045**	**0.0127**	**0.0113**	**0.00067**
	Error Trials: the distribution of phases is non-uniform	Mean ± 95% CI Phase (deg)	-94.3 ±37.1	110.19 ±53.2	-77.2 ±90	-73.9 ±90	-92.4 ±90	-131.8 ±90
		p-value	0.0642	0.1772	0.2716	0.0669	0.665	0.1732
Kuiper test	Error and correct trial distributions are the same	p-value	**0.005**	**0.002**	1	1	1	1

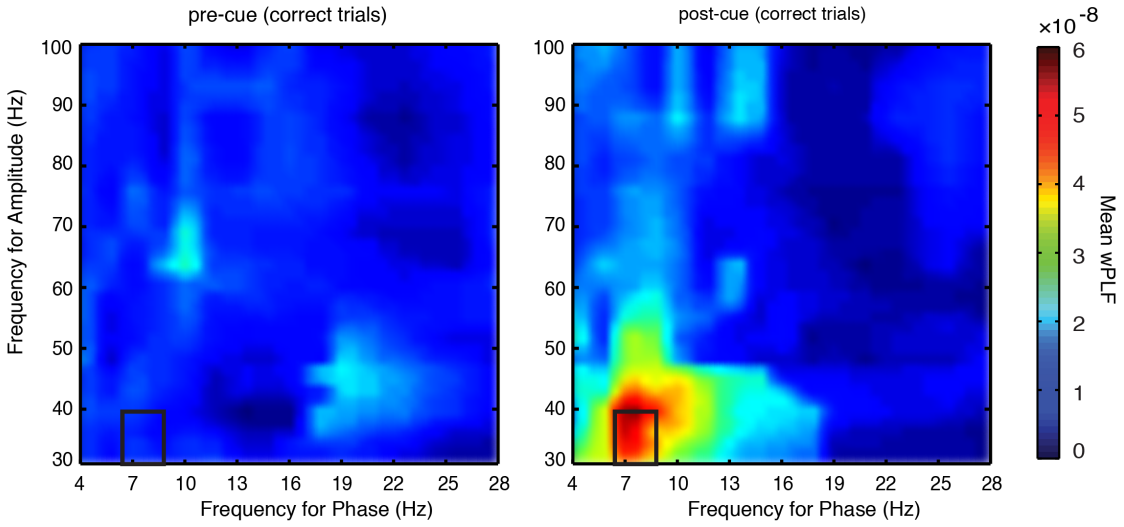

Figure A4. Theta-gamma correlation indexed with Maris' weighted phase Locking Factor
Comodulograms of average wPLF in the pre-cue (left panel) and post-cue (right panel) for the LFP-LFP pairs (n=85) that showed a significant increase ($p<0.05$) in coupling on correct trials. The black rectangle denotes frequency pairs that show a significant normalized difference in coupling at the population level.

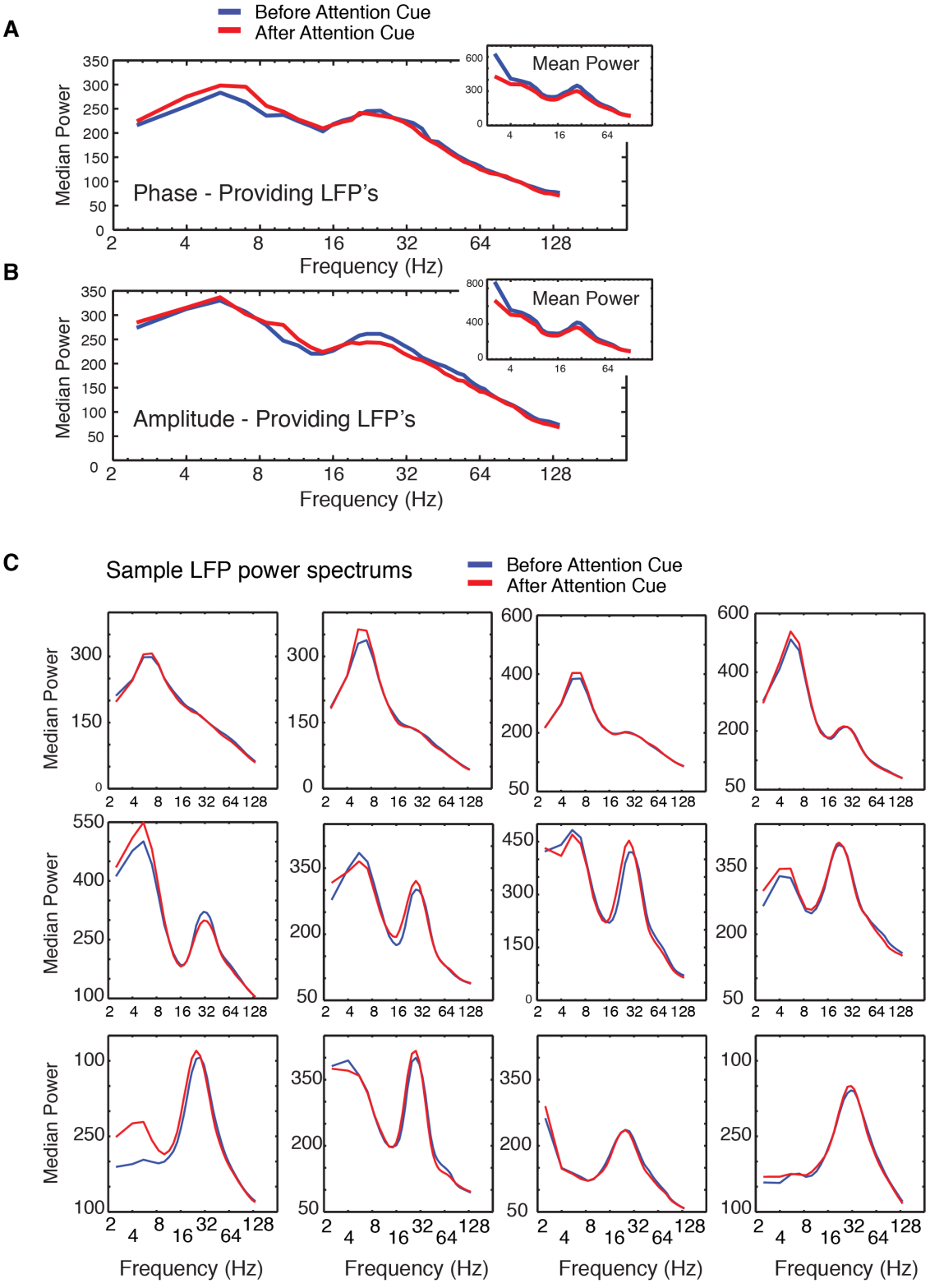
A
Before Attention Cue
After Attention Cue
Median Power
Mean Power
Phase - Providing LFP's
Frequency (Hz)
B
Median Power
Mean Power
Amplitude - Providing LFP's
Frequency (Hz)
C
Sample LFP power spectrums
Before Attention Cue
After Attention Cue
Median Power
Frequency (Hz)

Figure A5. Median power spectral densities for phase- and amplitude- providing LFP recordings

(**A**) Median power spectral density (*y-axis*) for unique LFP recordings (n=74) that provided the low frequency phase information to the LFP-LFP pairs that showed significant theta-gamma P-A correlation in the post-attention cue epoch but not in the pre-attention cue epoch. Line colors denote the median power in 500 ms time windows immediately before the attention cue (*blue*) and immediately after the attention cue onset (*red*). The inset shows the mean power spectral density instead of the median.

(**B**) Same format as (**A**) but in unique LFP recordings that provided the amplitude information (n=67) to the theta-gamma P -A correlation.

(C) Average power spectral densities (*y-axis*) for twelve example LFPs that engaged in significant cross frequency P-A correlation in the 500 ms after the onset of the attention cue (red), but not before the attention cue onset (blue). Power spectra were arranged so that LFPs with a stronger theta power component are shown earlier, and LFPs with relatively stronger beta LFP peak are shown later in the sequence. The examples illustrate the range of LFP power spectral densities evident in the PFC / ACC, and they show that there were no apparent LFP power modulations between the pre- and post- cue attention epoch.

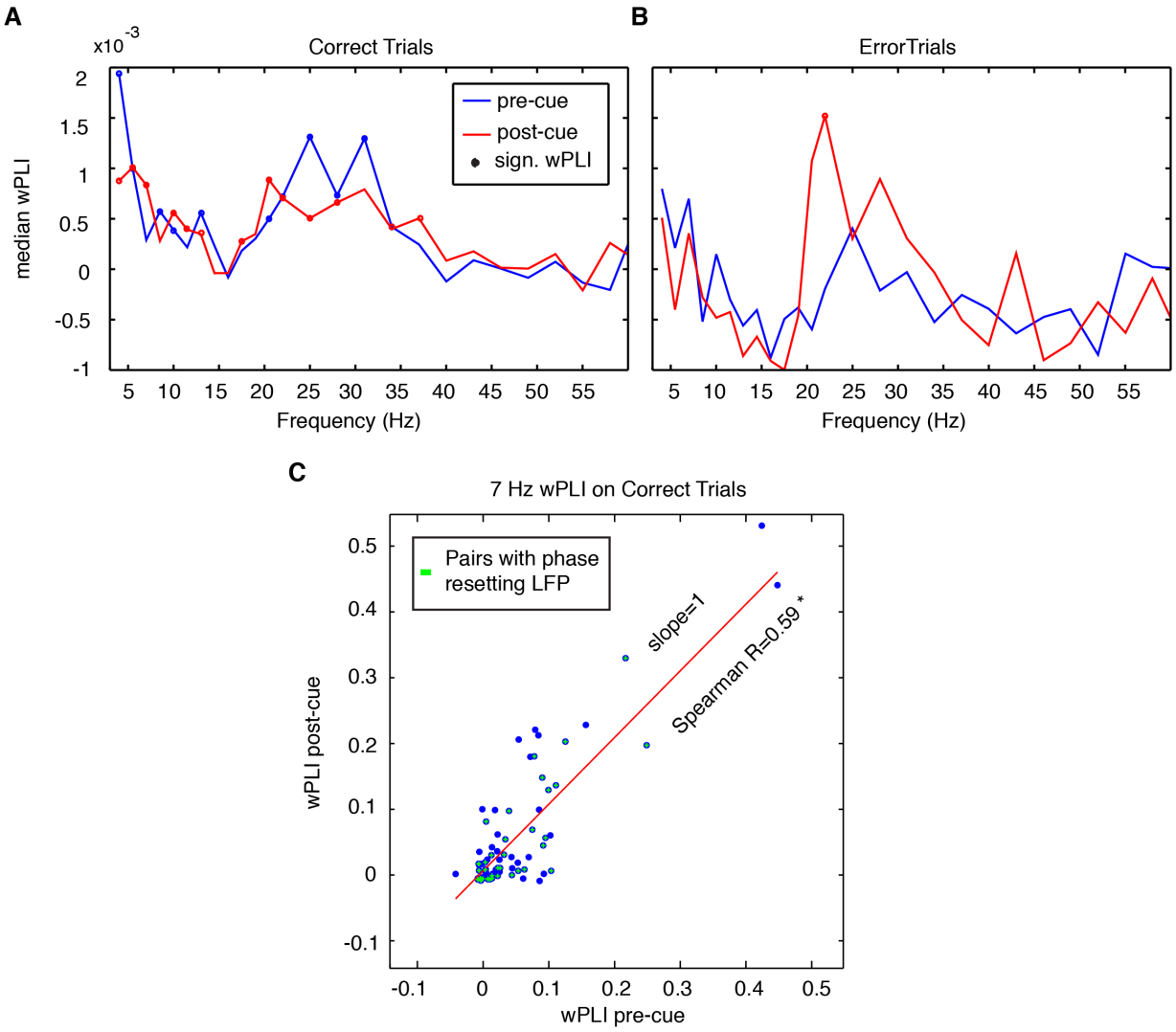

Figure A6. Phase synchronization in the phase-amplitude correlation network during the attention shift

(**A** and **B**) Average phase synchronization (measured as wPLI) across LFP pairs (n=85) that showed a reliable increase in phase-amplitude theta-gamma correlation, for correct (**A**) and error (**B**) trials. There was no significant change in phase synchronization between the pre- and post-cue epochs (see **Result A7**). The dots mark frequencies where the average wPLI was significantly higher than zero (Wilcoxon signrank).

(**C**) Spearman rank correlation and linear regression (red line) of the wPLI in the pre- and post-cue epoch. Spearman R was significant ($p<0.05$). Green crosses highlight those phase-amplitude correlation LFP pairs where the theta-providing LFP showed a significant phase reset 100-300 ms after attention cue onset. Phase resetting channels are broadly distributed even among weakly P-A correlated LFP pairs.

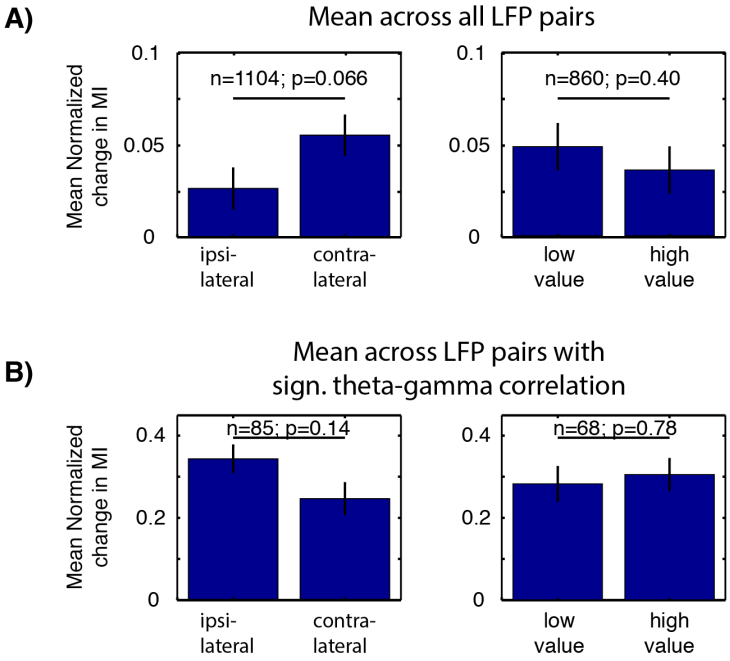

Figure A7. Representation of spatial information and information about target associated reward outcome in theta-gamma phase-amplitude correlation

(**A**) The average change in theta-gamma correlation across all LFP pairs for different spatial and reward outcome conditions (n=1104 for spatial conditions, n=860 for value conditions), represented as the mean and standard error There is a higher increase in correlation on contralateral vs ipsilateral trials (*left panel*), but no difference between attention to lower vs higher rewarded targets (*right panel*).

(**B**) Same as in (***A***), but only for LFP pairs where theta-gamma correlation showed reliable increase in the post-cue period (n=85 for spatial conditions, n=68 for value conditions). Insignificant theta-gamma correlation was masked to zero. There is no difference between contra- and ipsi-lateral trials, or between high and low value target trials.

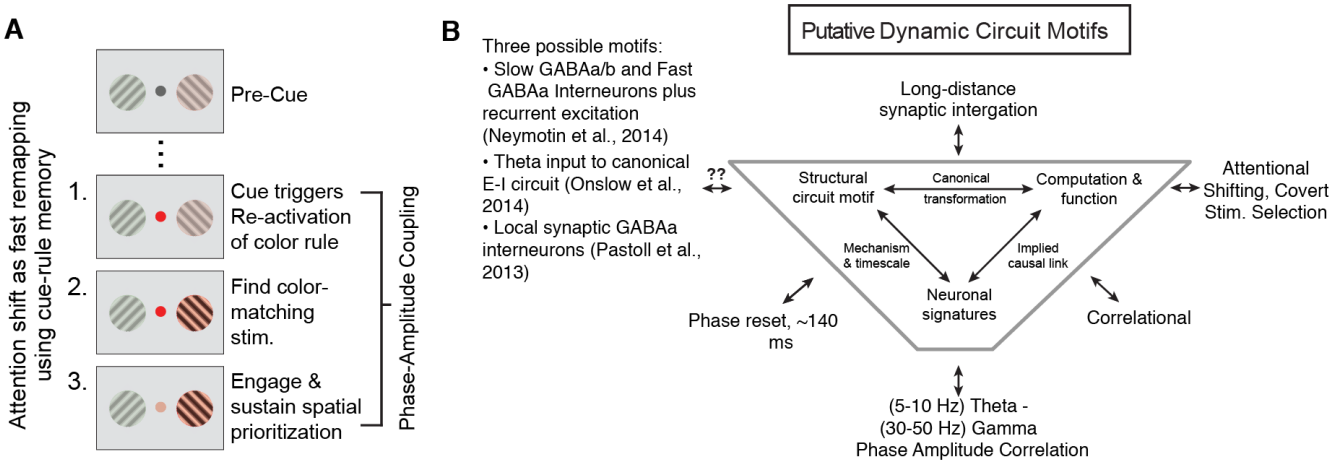

Figure A8. Cue triggered attention shifts during rule reactivation and remapping, and hypothetical dynamic circuit motif of theta-gamma P-A correlation

(**A**) Illustration of three separable component processes underlying the cue triggered (covert) attention shift. The panel shows the succession from pre-cue (top panel) to post-cue period (bottom three panels). The panels show that attention shifting proceeds from (1) the reactivation of a colour rule, (2) applying the rule by finding the color matching peripheral stimulus and filtering out non-matching stimuli, and (3) engaging and sustaining stimulus selection.

(**B**) The framework of the tripartite Dynamic Circuit Motifs helps understand how an activation signature (theta-gamma P-A correlation) links to a function (attentional shifting and stimulus selection). Completion of a dynamic motif would require identification of the structural (cellular and synaptic) origin of the activation state. (For details, *see* (Womelsdorf et al., 2014b)). The shown putative motif makes it explicit that the link of theta-gamma P-A correlation and attentional prioritization is correlational. Moreover, we can only speculate which synaptic or cellular mechanisms implement theta-gamma P-A correlation, but outlined are three generic cortical circuits that are powerful candidates.